AD-A157 809 A BRIEF INVESTIGATION OF ADAPTIVE DECISION FEEDBACK EQUALIZATION FOR DIGI..(U) MISSION RESEARCH CORP SANTA BARBARA CA B E SAWYER 01 NOV 83 MRC-R-801 DNA-6319T 1/1

UNCLASSIFIED DNA001-80-C-0022 F/G 9/5 NL

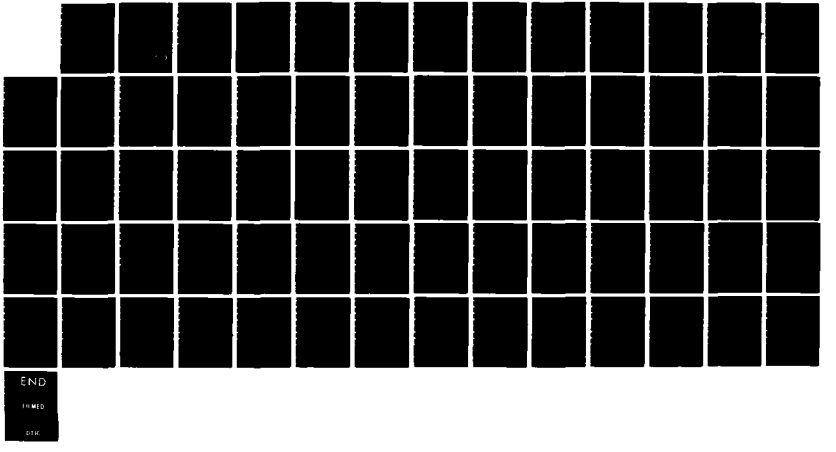

END

FILMED

DTIC

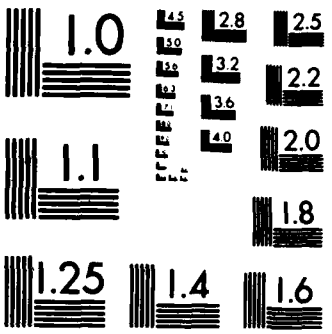

DNA 6319T

A BRIEF INVESTIGATION OF ADAPTIVE DECISION FEEDBACK EQUALIZATION FOR DIGITAL HF LINKS EMPLOYING PSK MODULATION

B.E. Sawyer
Mission Research Corporation
P.O. Drawer 719
Santa Barbara, CA 93102-0719

1 November 1983

Technical Report

CONTRACT No. DNA 001-80-C-0022

THIS WORK WAS SPONSORED BY THE DEFENSE NUCLEAR AGENCY
UNDER RDT&E RMSS CODE X322080469 Q94QAXHB05301 H2590D.

Prepared for
Director
DEFENSE NUCLEAR AGENCY
Washington, DC 20305-1000

Destroy this report when it is no longer needed. Do not return to sender.

PLEASE NOTIFY THE DEFENSE NUCLEAR AGENCY, ATTN: STTI, WASHINGTON, DC 20305-1000, IF YOUR ADDRESS IS INCORRECT, IF YOU WISH IT DELETED FROM THE DISTRIBUTION LIST, OR IF THE ADDRESSEE IS NO LONGER EMPLOYED BY YOUR ORGANIZATION.

UNCLASSIFIED

SECURITY CLASSIFICATION OF THIS PAGE *(When Data Entered)*

REPORT DOCUMENTATION PAGE		READ INSTRUCTIONS BEFORE COMPLETING FORM
1. REPORT NUMBER DNA 6319T	2. GOVT ACCESSION NO. AD-A157809	3. RECIPIENT'S CATALOG NUMBER
4. TITLE *(and Subtitle)* A BRIEF INVESTIGATION OF ADAPTIVE DECISION FEEDBACK EQUALIZATION FOR DIGITAL HF LINKS EMPLOYING PSK MODULATION		5. TYPE OF REPORT & PERIOD COVERED Technical Report 6. PERFORMING ORG. REPORT NUMBER MRC-R-801
7. AUTHOR(s) Blair E. Sawyer		8. CONTRACT OR GRANT NUMBER(s) DNA 001-80-C-0022
9. PERFORMING ORGANIZATION NAME AND ADDRESS Mission Research Corporation P.O. Drawer 719 Santa Barbara, California 93102-0719		10. PROGRAM ELEMENT, PROJECT, TASK AREA & WORK UNIT NUMBERS Task Q94QAXHB-05301
11. CONTROLLING OFFICE NAME AND ADDRESS Director Defense Nuclear Agency Washington, D.C. 20305-1000		12. REPORT DATE 1 November 1983 13. NUMBER OF PAGES 68
14. MONITORING AGENCY NAME & ADDRESS *(if different from Controlling Office)*		15. SECURITY CLASS *(of this report)* UNCLASSIFIED 15a. DECLASSIFICATION/DOWNGRADING SCHEDUL N/A since UNCLASSIFIED

16. DISTRIBUTION STATEMENT *(of this Report)*

Approved for public release; distribution is unlimited.

17. DISTRIBUTION STATEMENT *(of the abstract entered in Block 20, if different from Report)*

18. SUPPLEMENTARY NOTES

This work was sponsored by the Defense Nuclear Agency under RDT&E RMSS code X322080469 Q94QAXHB05301 H2590D.

19. KEY WORDS *(Continue on reverse side if necessary and identify by block number)*

PSK Receiver Mitigation
Adaptive Equalization
Decision Feedback Equalization
HF Communications

20. ABSTRACT *(Continue on reverse side if necessary and identify by block number)*

Adaptive decision feedback equalization is one of several mitigation techniques that can be employed to improve the performance of narrowband HF modems operating under time and frequency selective channel conditions. The decision feedback equalizer (DFE) is described and several adaptation algorithms are derived. Computer simulations of BPSK HF modems were used to compare link performance (in terms of bit error rate) with and without employment of an adaptive DFE. Also the performance was quantified versus channel disturbance parameters for a specific 2400 baud modem.

DD FORM 1 JAN 73 1473 EDITION OF 1 NOV 65 IS OBSOLETE

UNCLASSIFIED

SECURITY CLASSIFICATION OF THIS PAGE *(When Data Entered)*

TABLE OF CONTENTS

TABLE OF CONTENTS (Continued)

LIST OF ILLUSTRATIONS

SECTION 1
INTRODUCTION

Adaptive equalization is one of several mitigation schemes that can be designed into HF communication systems to combat the effects of frequency selective fading. Other possible schemes include maximum likelihood sequence estimation and various spread spectrum techniques. The restriction on the scope of this work to adaptive equalization should not be interpreted as a disparaging reflection upon the potential benefits of the other possibilities, but merely represents the limitations caused by time and resource constraints.

The use of adaptive equalization does not increase the bandwidth of the transmitted signal. Also, for the narrowband modulation type of interest here, PSK, long, deep fades can occur which span the modulation bandwidth. Thus one would envision an adaptive equalizer to be used in the context of HF transceivers having the capability to scan the HF band and to select and maintain a good carrier frequency automatically.

The particular type of equalizer addressed in this report is called a decision feedback equalizer (DFE), so named because decisions on the value of previously detected channel symbols are fed back to the equalizer to be incorporated into its internal state vector.

Section 2 of this report is meant to be a complete introduction to adaptive decision feedback equalization. By collecting the pertinent contents of several journal articles into this section the reader is freed from sorting through several sets of notation. Also all derivations in

Section 2 are generalized for fractionally-spaced sampling, coherent demodulation and time-variant channels, while the journal articles tend to address special cases. Of the numerous articles on adaptive equalization to be found in the open literature, three in particular are widely referenced, historically important, and pertinent to this report: Austin's derivation of the decision feedback equalizer from decision-theoretic principles (Reference 1); Gersho's treatment of the stochastic gradient algorithm in the context of linear equalization (Reference 2) which is easily extended to decision feedback equalization; and Godard's application of Kalman filtering principles to equalizer adaptation (Reference 3). In addition to these, References 4, 5, and 6 develop the fast Kalman adaptation algorithm. The derivation of the fast Kalman algorithm in Section 2 closely follows the treatment of transversal filter equalizer adaptation found in Reference 6, but extends the derivation to decision feedback equalizer adaptation using the mathematical tools provided by Reference 4.

The results obtained during this investigation were generated with a Monte Carlo computer simulation of an HF link. The computer simulation is described in Section 3, with primary emphasis given to the channel and receiver models.

Section 4 discusses the results of a simulation-aided analysis of HF PSK modems. First, the performance of conventional and equalizer-assisted modems are compared for a simple time-invariant HF channel model. Then an equalizer-assisted modem is analyzed for a simple time-varying frequency-selective HF channel model.

SECTION 2
ADAPTIVE DECISION FEEDBACK EQUALIZATION

A decision feedback equalizer (DFE) is a digital signal processor that can enhance the performance of several types of digital modems operating under frequency selective channel conditions. This discussion is generalized to include T/N sampling, phase coherent demodulation and random channel variability. T/N sampling means the receiver samples the analog channel output every T/N seconds where T is the minimum signaling interval of the modulated waveform. Phase coherent demodulation means the demodulator uses phase as well as amplitude information, which implies the DFE must process complex numerical data. Random channel variability means the channel transfer function is time-variant and is unknown a priori to the receiver, which implies the DFE must be able to continuously adapt its internal parameters to match the channel.

Two adaptation techniques commonly discussed in the technical literature are the fast Kalman and the stochastic gradient algorithms. Both of the algorithms have larger implementation requirements than the DFE itself. The fast Kalman algorithm requires more hardware and/or digital processing than that required to implement the stochastic gradient algorithm. However, the fast Kalman algorithm converges faster than the stochastic gradient algorithm.

We shall first discuss a baseband channel representation that is appropriate for several digital modulation schemes, and then describe the T/N fractionally-spaced DFE. The remainder of this report formulates several adaptation techniques starting with the stochastic gradient algorithm. Then various least square adaptation algorithms shall be derived, culminating with the fast Kalman algorithm.

2.1 BASEBAND CHANNEL MODEL

It is convenient to model the modulation, channel propagation and demodulation processes with a time-discrete complex baseband (or analytic signal) representation. Such a representation of the modulated waveform is the sequence of complex samples $\{d_k\}$. The transmitted waveform represented by the discrete sequence $\{d_k\}$ is of the form

$$\sum_{k=0}^{\infty} [\text{Real}(d_k) \cos(\omega_c t) + \text{Imag}(d_k) \sin(\omega_c t)] \text{ rect } (t/T_s - k)$$

where ω_c is the carrier frequency, T_s is the sampling interval, and the rect function is defined as

$$\text{rect } (X) = \begin{cases} 1 & -1/2 < X \leq 1/2 \\ 0 & \text{otherwise .} \end{cases}$$

Several quadrature amplitude modulation (QAM) and M-ary phase shift keying (PSK) modulation types can be represented with this discrete baseband formulation by appropriately selecting the alphabet for d_k. For example, limiting d_k to the set $\{1,-1\}$ would correspond to BPSK modulation. Also, T/N spaced sampling is represented by only changing d_k every N samples, in which case $T_s = T/N$. We shall use the convention that the receiver generates a detected symbol when k is an integer multiple of N.

The time-discrete analytic signal representation of the channel at the k^{th} sample time is the set of complex samples $\{h_k^m\}$, the sampled-data response of the channel to an isolated unit sample. More specifically, suppose that d_n is one and d_k is zero for all k not equal to n. Then the discrete channel output (ignoring noise) at the kth sample time is

h_k^{k-n-M}. The integer M corresponds to the propagation delay and is used here as a convenience so that we can require h_k^m equal to zero for $m < 0$, since the channel is causal and hence M must be non-negative. It is further assumed that the channel has finite memory, and we introduce L, called the channel memory duration, which is the smallest integer such that h_k^m is zero for all $m > L$. For our purposes the values h_k^m in the range $0 \leq m \leq L$ completely specify the intersymbol interference characteristics of the channel and are used to form the vector $\underline{h}_k$.

$$\underline{h}_k^T \triangleq [h_k^0 \quad h_k^1 \quad h_k^2 \ldots h_k^L].$$

The underbar denotes a column vector and superscript T denotes vector transpose. The transpose form is used for typographical simplicity because it allows the column vectors to be presented in a horizontal orientation. Next we define a vector of the most recent L+1 channel symbols.

$$\underline{d}_k^T = [d_k \quad d_{k-1} \quad d_{k-2} \ldots d_{k-L}] \tag{1}$$

The k^{th} received sample constituting the output of the discrete channel, denoted u_k, is the convolution of the unit sample response with a sequence of inputs, corrupted by additive noise.

$$u_k \triangleq \underline{h}_k^T \underline{d}_k + n_k = \sum_{m=0}^{L} h_k^m d_{k-m} + n_k \tag{2}$$

n_k is the complex white gaussian noise component received during the k^{th} sampling interval. A block diagram of the tapped delay line implementation of the baseband channel model is shown in Figure 1.

1) A linear forward predictor of the next N+1 samples to enter $\underline{x}_k$ is derived. This forward predictor uses $\underline{g}_k$, the same Kalman gain vector of an LS algorithm adapting a DFE.

2) A linear backward predictor of the last N+1 samples to leave $\underline{x}_k$ is derived. This backward predictor also uses $\underline{g}_k$.

3) LS adaptation is applied to an extended state DFE to develop the mathematical structure between the forward and backward predictors.

4) It is shown that the forward and backward predictors can work in tandem to efficiently calculate $\underline{g}_k$ recursively.

2.6.1 Forward Prediction

Define a vector $\underline{\xi}_k$ composed of the N+1 elements entering the state vector at the k^{th} sample time when k/N is an integer.

$$\underline{\xi}_k^T \triangleq [u_k \; u_{k-1} \cdots u_{k-N+1} \; d_{k-D-N}] \tag{39}$$

The linear prediction of $\underline{\xi}_{k+N}$ is $F_{k-N}^{*} \underline{x}_k$ where F_k is an (N+1) x (K_1+1+K_2) rectangular matrix of forward prediction coefficients. The forward prediction error vector is defined as

$$\underline{f}_k \triangleq \underline{\xi}_{k+N} - F_{k-N}^{*} \underline{x}_k \; . \tag{40}$$

A comparison of this equation with Equation (21) shows a similarity between this forward predictor and the DFE. To calculate the optimal value of F_k, the scalar error LS cost function of Equation (8) is generalized for vector errors.

The sequence of operations performed by this algorithm after the k^{th} sample time (when k/N is an integer) is

$$\underline{t}_k \triangleq T_{k-N}\, \underline{x}_k \tag{34}$$

[33,34] $$\underline{g}_k = \underline{t}_k / (\lambda + \underline{x}_k^* \underline{t}_k) \tag{35}$$

[30,34, 35] $$T_k = \frac{1}{\lambda} [T_{k-N} - \underline{g}_k \underline{t}_k^*] \tag{36}$$

[21] $$\varepsilon_k = d_{k-D} - \underline{c}_{k-N}^* \underline{x}_k \tag{37}$$

[23] $$\underline{c}_k = \underline{c}_{k-N} + \underline{g}_k \varepsilon_k^* . \tag{38}$$

The implementation complexity of this algorithm can be dominated by the first step which requires $(K_1+1+K_2)^2$ multiplications. The following algorithm is equivalent to this one, but is computationally superior because it manipulates smaller matrices.

2.6 THE FAST KALMAN ADAPTATION ALGORITHM

None of the adaptation algorithms discussed thus far take into consideration any deterministic relationship between $\underline{x}_k$ and $\underline{x}_{k-N}$. From the definition of $\underline{x}_k$ in Equation (5), all but N+1 of the elements in $\underline{x}_{k-N}$ also reside in $\underline{x}_k$. The fast Kalman algorithm attains its computational efficiency by exploiting this fact.

The derivation of the fast Kalman Algorithm will proceed as follows:

Since $\lambda + \underline{x}_k A_{k-N}^{-1} \underline{x}_k$ is a scalar and A_k is invertible,

[28] $$A_k^{-1} = \frac{1}{\lambda}\left[A_{k-N}^{-1} - \frac{A_{k-N}^{-1}\underline{x}_k \underline{x}_k^* A_{k-N}^{-1}}{\lambda + \underline{x}_k^* A_{k-N}^{-1}\underline{x}_k}\right]. \qquad (29)$$

Define $T_k = A_k^{-1}$ and notice that T_k like A_k is hermitian since

$$T_k^T A_k^T = (A_k T_k)^T = I = (A_k T_k)^* = T_k^* A_K^* = T_K^* A_K^T$$

and postmultiplication by the inverse of A_k^T implies that T_k^T equals T_k^*. Substituting T_k into Equation (29) yields the following formula.

[29] $$T_k = \frac{1}{\lambda}\left[T_{k-N} - \frac{T_{k-N}\underline{x}_k \underline{x}_k^* T_{k-N}}{\lambda + \underline{x}_k^* T_{k-N}\underline{x}_k}\right]. \qquad (30)$$

Now consider $\underline{g}_k$.

[19] $$\underline{g}_k = A_k^{-1}\underline{x}_k = T_k \underline{x}_k \qquad (31)$$

[30,31] $$\underline{g}_k = \frac{1}{\lambda}\left[T_{k-N}\underline{x}_k - \frac{T_{k-N}\underline{x}_k \underline{x}_k^* T_{k-N}\underline{x}_k}{\lambda + \underline{x}_k^* T_{k-N}\underline{x}_k}\right] \qquad (32)$$

[32] $$\underline{g}_k = \frac{T_{k-N}\underline{x}_k}{\lambda + \underline{x}_k^* T_{k-N}\underline{x}_k} \qquad (33)$$

2.5 THE KALMAN ADAPTATION ALGORITHM

First we shall derive a recursive calculation of A_k^{-1} from which a recursive formula for $\underline{g}_k$ will easily follow. This algorithm bypasses the necessity of matix inversion, and as a result is more efficient than the one discussed immediately above.

It is easy to verify the following equation.

$$A_{k-N}^{-1}\,\underline{x}_k\,\lambda^{-1}\,\underline{x}_k^* = A_{k-N}^{-1}\,\underline{x}_k\,\lambda^{-1}\,[\lambda + \underline{x}_k^*\,A_{k-N}^{-1}\,\underline{x}_k]\,[\lambda + \underline{x}_k^*\,A_{k-N}^{-1}\,\underline{x}_k]^{-1}\,\underline{x}_k^* \tag{24}$$

[24] $$A_{k-N}^{-1}\,\underline{x}_k\,\lambda^{-1}\,\underline{x}_k^* = A_{k-N}^{-1}\,\underline{x}_k\,[\lambda + \underline{x}_k^*\,A_{k-N}^{-1}\,\underline{x}_k]^{-1}\,\underline{x}_k^* + A_{k-N}^{-1}\,\underline{x}_k\,\lambda^{-1}\,\underline{x}_k^*\,A_{k-N}^{-1}\,\underline{x}_k\,[\lambda + \underline{x}_k^*\,A_{k-N}^{-1}\,\underline{x}_k]^{-1}\,\underline{x}_k^* \tag{25}$$

[25] $$I = [I + A_{k-N}^{-1}\,\underline{x}_k\,\lambda^{-1}\,\underline{x}_k^*]\,[I - A_{k-N}^{-1}\,\underline{x}_k(\lambda + \underline{x}_k^*\,A_{k-N}^{-1}\,\underline{x}_k)^{-1}\,\underline{x}_k^*] \tag{26}$$

Postmultiply by A_{k-N}^{-1} and premultiply by A_{k-N}

[26] $$I = [A_{k-N} - \underline{x}_k\,\lambda^{-1}\,\underline{x}_k^*]\,[A_{k-N}^{-1} - A_{k-N}^{-1}\,\underline{x}_k\,(\lambda + \underline{x}_k^*\,A_{k-N}^{-1}\,\underline{x}_k)^{-1}\,\underline{x}_k^*\,A_{k-N}^{-1}] \tag{27}$$

[13,27] $$I = \frac{1}{\lambda}\,A_k\,[A_{k-N}^{-1} - A_{k-N}^{-1}\,\underline{x}_k\,(\lambda + \underline{x}_k^*\,A_{k-N}^{-1}\,\underline{x}_k)^{-1}\,\underline{x}_k^*\,A_{k-N}^{-1}]\,. \tag{28}$$

The recursive calculation of $\underline{c}_k$ is now derived.

[10,14] $$A_k \underline{c}_k = \lambda A_{k-N} \underline{c}_{k-N} + \underline{x}_k d^*_{k-D} \tag{15}$$

[13,15] $$A_k \underline{c}_k = (A_k - \underline{x}_k \underline{x}^*_k) \underline{c}_{k-N} + \underline{x}_k d^*_{k-D} \tag{16}$$

[16] $$A_k \underline{c}_k = A_k \underline{c}_{k-N} + \underline{x}_k (d_{k-D} - \underline{c}^*_{k-N} \underline{x}_k)^* \tag{17}$$

Premultiply by A_k^{-1}

[17] $$\underline{c}_k = \underline{c}_{k-N} + \underline{g}_k (d_{k-D} - \underline{c}^*_{k-N} \underline{x}_k)^* \tag{18}$$

where $$\underline{g}_k \triangleq A_k^{-1} \underline{x}_k \quad . \tag{19}$$

The sequence of operations of this recursive algorithm after the k^{th} sample time is

[13] $$A_k = \lambda A_{k-N} + \underline{x}_k \underline{x}^*_k \tag{20}$$

$$\varepsilon_k = d_{k-D} - \underline{c}^*_{k-N} \underline{x}_k \tag{21}$$

[19] $$\underline{g}_k = A_k^{-1} \underline{x}_k \tag{22}$$

[18,21] $$\underline{c}_k = \underline{c}_{k-N} + \underline{g}_k \varepsilon^*_k \quad . \tag{23}$$

Notice that the calculation of A_k and $\underline{c}_k$ is greatly simplified and that the calculation of the quantity $\underline{v}_k$ has been bypassed altogether. However, A_k must be inverted to calculate $\underline{g}_k$ and the dimension of A_k is K_1+1+K_2, often a large number. The calculation of g_k can also be done recursively, and algorithms that do so are discussed in the next two sections.

[8] $$\left(\sum_{n=0}^{k/N} \lambda^{n-k/N}\ \underline{x}_{nN}\ \underline{x}^{*}_{nN}\right)\ \underline{c}_k = \left(\sum_{n=0}^{k/N} \lambda^{n-k/N}\ \underline{x}_{nN}\ d^{*}_{nN-D}\right) \qquad (9)$$

The quantity on the right is a column vector and the quantity premultiplying $\underline{c}_k$ on the left is a positive-definite hermitian square matrix. Some of the forthcoming derivations are tedious. To simplify the presentations, the numbers of preceding equations justifying a new expression are listed in brackets to the left, as was done above. Equation (9) can be restated as

[9] $$A_k\ \underline{c}_k = \underline{v}_k \qquad (10)$$

where

[9,10] $$A_k = \sum_{n=0}^{k/N} \lambda^{n-k/N}\ \underline{x}_{nN}\ \underline{x}^{*}_{nN} \qquad (11)$$

[9,10] $$\underline{v}_k = \sum_{n=0}^{k/N} \lambda^{n-k/N}\ \underline{x}_{nN}\ d^{*}_{nN-D} \qquad (12)$$

The recursive nature of Equations (11) and (12) is apparent and can be written as

[11] $$A_k = \lambda\ A_{k-N} + \underline{x}_k\ \underline{x}^{*}_k \qquad (13)$$

[12] $$\underline{v}_k = \lambda\ \underline{v}_{k-N} + \underline{x}_k\ d^{*}_{k-D} \qquad (14)$$

A new coefficient vector is calculated after each equalizer operation. Thus at the k^{th} sample time the quantities A_{k-N}, $\underline{v}_{k-N}$ and $\underline{c}_{k-N}$ are available so that A_k, $\underline{v}_k$ and $\underline{c}_k$ may be calculated recursively.

2.4 LEAST SQUARES ADAPTATION AND THE WIENER-HOPF EQUATIONS

The stochastic gradient algorithm discussed above was based upon the least mean square (LMS) cost function. Now we turn our attention to algorithms that minimize the least squares (LS) cost function given by

$$\text{LS cost function} = \sum_{n=0}^{k/N} \lambda^{n-k/N} \left| d_{nN-D} - \underline{c}_k^* \underline{x}_{nN} \right|^2 . \qquad (8)$$

This cost function is the geometrically weighted sum of the squared magnitude of all equalizer output errors if the equalizer coefficient vector had always been equal to $\underline{c}_k$. After the k^{th} equalizer output has been generated, the least squares adaptation algorithms generate the value of $\underline{c}_k$ that minimizes the LS cost function. As done previously, the discrete independent temporal index k increments with each received sample and hence increases by N with each equalizer operation. All quantities discussed henceforth are defined only when k/N is an integer. Thus, the previous value of quantities that change only after each equalizer operation are denoted with the subscript k-N instead of k-1.

For time invariant channels the selection of $\underline{c}_k$ should depend as much on previous data as current data, in which case the constant parameter λ appearing in the cost function should be unity. λ is incorporated into the LS cost function to allow for time varying channels. A real positive value of λ slightly smaller than unity causes received data to be less influential as it becomes older.

The optimal value of $\underline{c}_k$ is found by setting the gradient of the LS cost function with respect to $\underline{c}_k$ to zero which yields the discrete Wiener-Hopf equations.

Algorithm No. 1. An adaptive T/N fractionally-spaced DFE (stochastic gradient algorithm.

Step Number	Operation	Comment
1	$k \leftarrow 0$ $\underline{x}_{-N} \leftarrow \underline{0}$ $\underline{c}_{-N} \leftarrow \underline{0}$	Initialization
2	$\underline{x}_k \leftarrow S\,\underline{x}_{k-N} + P \begin{bmatrix} u_k \\ u_{k-1} \\ \cdot \\ \cdot \\ \cdot \\ u_{k-N+1} \end{bmatrix} + \underline{a}\, d_{k-D-N}$	Shift N new channel samples and previous decision sample into state vector
3	$y_k \leftarrow \underline{c}_{k-N}\,\underline{x}_k$	Equalization
4	$\underline{c}_k \leftarrow \underline{c}_{k-N} + \Delta\,(d_{k-D} - y_k)^*\,\underline{x}_k$	Adaptation
5	$k \leftarrow k + N$	Transition to next set of N input samples
6	Go back to step 2	

Each term in this equation can be readily derived.

$$\bar{\nabla} \left| d_{k-D} \right|^2 = \underline{0}$$

$$\bar{\nabla} \left| \underline{c}^*_{k-N} \underline{x}_k \right|^2 = 2 \underline{x}_k \underline{x}^*_k \underline{c}_{k-N} = 2 \underline{x}_k y^*_k$$

$$\bar{\nabla} \{ d^*_{k-D} \underline{c}^*_{k-N} \underline{x}_k + d_{k-D} (\underline{c}^*_{k-N} \underline{x}_k)^* \} = 2 d^*_{k-D} \underline{x}_k$$

Therefore

$$\bar{\nabla} \left| \varepsilon_k \right|^2 = -2 (d^*_{k-D} - y^*_k) \underline{x}_k = -2 \varepsilon^*_k \underline{x}_k$$

Then the stochastic gradient adaptation rule becomes:

$$\underline{c}_k \leftarrow \underline{c}_{k-N} + \Delta \varepsilon^*_k \underline{x}_k \tag{7}$$

To state the operation of a T/N fractionally-spaced DFE using the stochastic gradient adaptation algorithm we define a square matrix and a column vector both of dimension K_1+1+K_2 and a rectangular matrix having dimensions $(K_1+1+K_2) \times N$

$$S \triangleq \begin{bmatrix} & & \overbrace{\quad}^{N} & \overbrace{\quad}^{1} & \\ & & & & \} N \\ & I_{K_1+1-N} & & & \\ & & & & \} 1 \\ & & & I_{K_2-1} & \end{bmatrix} \qquad P \triangleq \begin{bmatrix} I_N \\ \hline \\ \\ \end{bmatrix}$$

$$\underline{a}^T \triangleq [0\ 0\ \ldots\ 0\ \underset{\text{(}K_1+2\text{)}^{th}\text{ element}}{1}\ 0\ \ldots\ 0]$$

All unlabeled partitions contain zero elements only. I denotes the identity matrix with dimension specified by the subscript. The adaptive equalizer operation is given by Algorithm 1.

This shall be done using a numerical search technique based upon the method of steepest descent called the stochastic gradient algorithm. The stochastic gradient iteration rule is

$$\underline{c}_k \leftarrow \underline{c}_{k-N} - 1/2\ \Delta\ \bar{\nabla} \left|\varepsilon_k\right|^2 \quad . \tag{6}$$

$\bar{\nabla} \left|\varepsilon_k\right|^2$ denotes the approximation of the gradient of $\left|\varepsilon_k\right|^2$ with respect to $\underline{c}_{k-N}$ where the slight dependence of $\underline{c}_{k-N}$ on d_{k-D} and $\underline{x}_k$ is ignored. Δ is a real scalar controlling algorithm performance, and the factor 1/2 is introduced here for later notational convenience. The use of the term "gradient" conforms to the nomenclature of common engineering practice and the technical literature. However, such usage is mathematically imprecise because the gradient of any real-valued function with respect to a complex valued vector either does not exist or is identically zero. To eliminate confusion the reader must interpret the gradient of a real-valued function with respect to a complex-valued vector as the sum of 1) the gradient of the real-valued function with respect to the real part of the complex vector and 2) the product of the square root of -1 and the gradient of the real-valued function with respect to the imaginary part of the complex vector.

The gradient of $\left|\varepsilon_k\right|^2$ at $\underline{c}_{k-N}$ points in the direction of maximum increase of $\left|\varepsilon_k\right|^2$. The stochastic gradient algorithm attempts to minimize $\left|\varepsilon_k\right|^2$ by perturbing $\underline{c}_{k-N}$ in the direction approximately opposite that of this gradient after each equalizer operation. To derive $\bar{\nabla} \left|\varepsilon_k\right|^2$, first expand $\left|\varepsilon_k\right|^2$.

$$\bar{\nabla} \left|\varepsilon_k\right|^2 = \bar{\nabla} \left\{ \left(d_{k-D} - \underline{c}^*_{k-N}\, \underline{x}_k\right) \left(d_{k-D} - \underline{c}^*_{k-N}\, \underline{x}_k\right)^* \right\}$$

$$= \bar{\nabla} \left|d_{k-D}\right|^2 + \bar{\nabla} \left|\underline{c}^*_{k-N}\, \underline{x}_k\right|^2 +$$

$$- \bar{\nabla} \left\{ d^*_{k-D}\, \underline{c}^*_{k-N}\, \underline{x}_k + d_{k-D} \left(\underline{c}^*_{k-N}\, \underline{x}_k\right)^* \right\} .$$

not have a priori knowledge of d_{k-D-N}, in which case the decision symbol $\hat{d}_{k-D-N}$ is based upon the equalizer output y_{k-N}. However, to simplify our consideration of the adaptation algorithms we shall assume that knowledge of d_{k-D-N} is available to the receiver. The complex tap weights of the feedforward section are chosen to coherently combine all the signal components of the received data arising from the transmission of d_{k-D} and can be viewed as a transversal filter qualitatively matched to the discrete channel unit sample response. This linear combination of the received data symbols will also have signal components arising from transmitted channel symbols other than d_{k-D}, half of which were transmitted prior to and half after d_{k-D}. Presumably, those transmitted prior to d_{k-D} have already been detected correctly. Hence the associated intersymbol interference (ISI) components in the weighted sum of the received data are deterministically related to the previous decision symbols. The coefficients of the feedback section, then, are selected to cancel these components. For the T/N fractionally-spaced DFE, L/N previously detected symbols are contributing ISI components to the weighted sum of the feedforward taps, and hence K_1 should be set equal to L and K_2 should be set approximately equal to L/N.

2.3 STOCHASTIC GRADIENT ALGORITHM

Define the error in the k^{th} equalizer output as $\varepsilon_k = d_{k-D} - y_k$, where the availability of d_{k-D} is assumed. One would like to iterate $\underline{c}_k$ to eventually drive ε_k to zero, but ε_k cannot completely diminish due to the random noise component in y_k. Failing that, it is desirable and mathematically convenient to have the adaptation algorithm try to minimize the least mean square (LMS) cost function.

$$\text{LMS cost function} = E\{|\varepsilon_k|^2\}$$

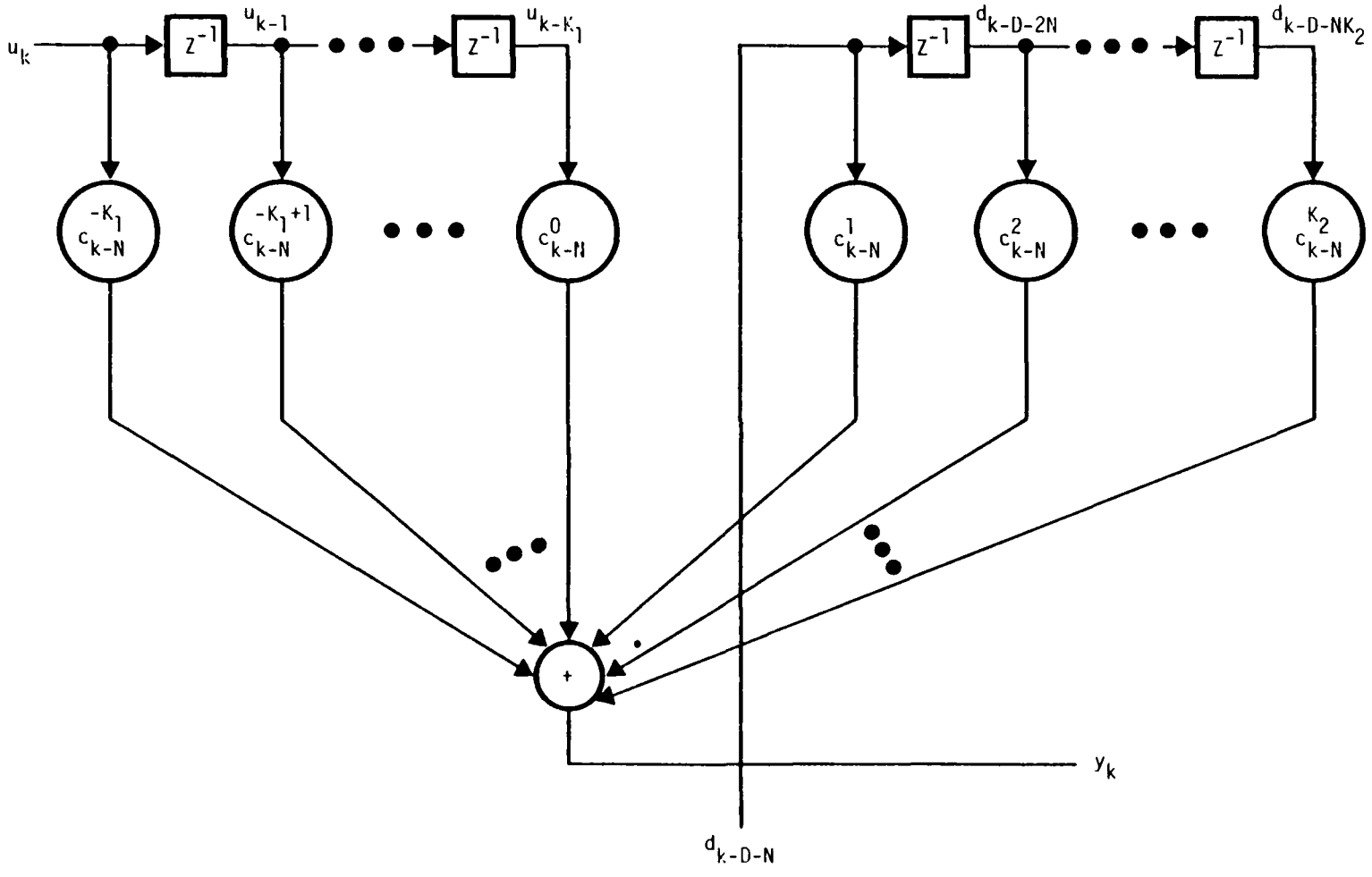

Figure 2. Block diagram of T/N fractionally-spaced decision feedback equalizer.

2.2 THE T/N FRACTIONALLY SPACED DFE

According to the definitions given above, a particular transmitted channel symbol d_{k-L} influences the currently received channel symbol u_k and previously received symbols $u_{k-1}, u_{k-2}, \ldots, u_{k-L}$. An equalizer ideally uses all of these received symbols to assist the receiver in generating the decision symbol $\hat{d}_{k-L}$, the receiver's estimate of d_{k-L}. As mentioned earlier, the values of d_k change at most every N samples, and the receiver generates a decision symbol only when k/N is an integer. To do this the equalizer actually processes the currently received symbol and the K_1 previously received symbols, where K_1 is chosen to be greater than or equal to L. A DFE processes K_2 past decision symbols also. After the k^{th} sample time the decision d_{k-D} is made, and the integer D must be in the range $L \leq D \leq K_1$ for proper equalizer operation. y_k denotes the DFE output generated after the k^{th} sample and is calculated by

$$y_k = \underline{c}^*_{k-N}\, \underline{x}^*_k \qquad \text{(* denotes conjugate transpose)} \qquad (3)$$

$$\text{where} \quad \underline{c}^*_k \triangleq [c_k^{-K_1}\ c_k^{-K_1+1} \cdots c_k^{-1}\ c_k^0\ c_k^1 \cdots c_k^{K_2}] \qquad (4)$$

$$\text{and} \quad \underline{x}^T_k \triangleq [u_k\ u_{k-1} \cdots u_{k-K_1}\ d_{k-D-N}\ d_{k-D-2N} \cdots d_{k-D-NK_2}] \qquad (5)$$

The mechanization of this calculation is shown in Figure 2. $\underline{x}_k$ is called the state vector and $\underline{c}_{k-N}$ the coefficient vector. The elements of $\underline{c}_{k-N}$ are the tap weights shown in the block diagram. For this coherent baseband implementation of the equalizer, these coefficients are complex scalars.

The block diagram indicates the DFE can be implemented as two tapped delay lines. The one on the left is called the feedforward section and the one on the right the feedback section. Usually the receiver does

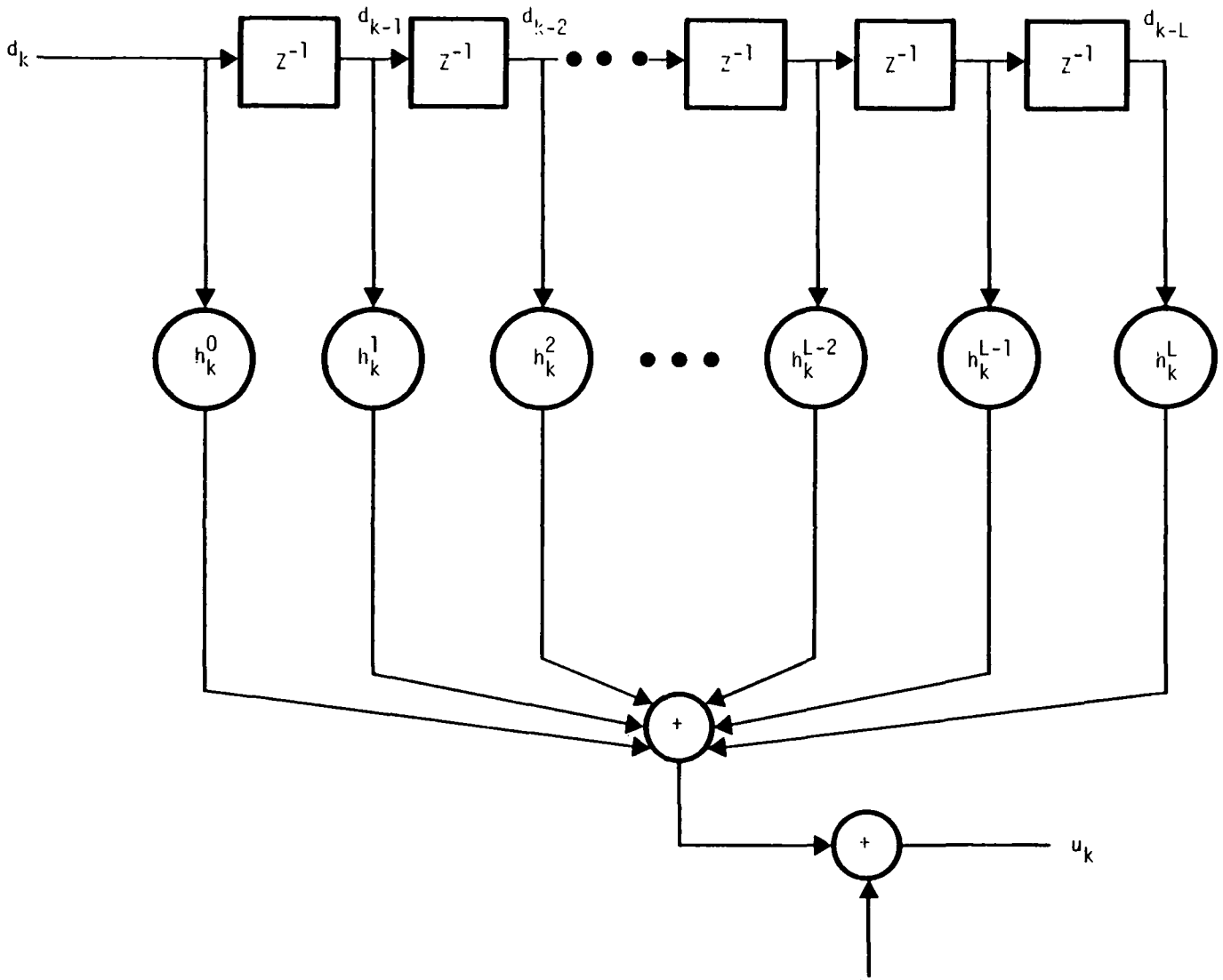

Figure 1. Block diagram of discrete baseband channel model.

$$\text{forward prediction LS cost function} = \sum_{n=0}^{k/N} \lambda^{n-k/N} \left(\underline{\xi}_{nN+N} - F_k^* \underline{x}_{nN}\right)\left(\underline{\xi}_{nN+N} - F_k^* \underline{x}_{nN}\right)^* \tag{41}$$

Each column of F_k contains all the coefficients used to predict a single element within $\underline{\xi}_{k-N}$. The Wiener-Hopf equations yielding the optimal F_k are found by setting to zero the gradient of the trace of the LS cost function with respect to each column of F_k. The result is

[41] $$\left(\sum_{n=0}^{k/N} \lambda^{n-k/N} \underline{x}_{nN} \underline{x}_{nN}^*\right) F_k = \sum_{n=0}^{k/N} \lambda^{n-k/N} \underline{x}_{nN} \underline{\xi}_{nN}^* \tag{42}$$

or

[11,42] $$A_k F_k = V_k^f \tag{43}$$

where

[42,43] $$V_k^f \triangleq \sum_{n=0}^{k/N} \lambda^{n-k/N} \underline{x}_{nN} \underline{\xi}_{nN+N}^* = \lambda V_{k-N}^f + \underline{x}_k \underline{\xi}_{k+N}^* \,. \tag{44}$$

Repeating the manipulations of Equations (15) through (19) using F_{k-N} and $\underline{\xi}_{k+N}$ instead of $\underline{c}_{k-N}$ and d_{k-D} yields

[18] $$F_k = F_{k-N} + g_k \left(\underline{\xi}_{k+N} - F_{k-N}^* \underline{x}_k\right)^* \tag{45}$$

[40,45] $$F_k = F_{k-N} + \underline{g}_k \underline{f}_k^* \tag{46}$$

Now we define the minimum value of the LS cost function given by Equation (41) as E_k^f, which is found by substituting Equation (43) into Equation (41) and simplifying.

[11,42, 43,44] $$E_k^f = R_k^f - V_k^{f*} F_k \tag{47}$$

where

$$R_k^f \triangleq \sum_{n=0}^{k/N} \lambda^{n-k/N} \underline{\xi}_{nN+N} \underline{\xi}_{nN+N}^* = \lambda R_{k-N}^f + \underline{\xi}_{k+N} \underline{\xi}_{k+N}^* \quad . \tag{48}$$

A recursive calculation of E_k^f is now derived.

[44,46, 47,48] $$E_k^f = \lambda R_{k-N}^f + \underline{\xi}_{k+N} \underline{\xi}_{k+N}^* - (\lambda V_{k-N}^f + \underline{x}_k \underline{\xi}_{k+N}^*)^* (F_{k-N} + \underline{g}_k f_k^*) \tag{49}$$

[40,46, 49] $$E_k^f = \lambda(R_{k-N}^f - V_{k-N}^{f*} F_{k-N}) + (\underline{f}_k + F_{k-N}^* \underline{x}_k)(f_k + F_{k-N}^* \underline{x}_k)^* - \lambda V_{k-N}^{f*} \underline{g}_k \underline{f}_k^* - \underline{\xi}_{k+N} \underline{x}_k^* F_k \tag{50}$$

[40,44, 47,50] $$E_k^f = \lambda E_{k-N}^f + \underline{\xi}_{k+N} \underline{x}^* (F_{k-N} - F_k) + \underline{f}_k \underline{f}_k^* + F_{k-N}^* \underline{x}_k \underline{f}_k^* - (V_k^{f*} - \underline{\xi}_{k+N} \underline{x}_k^*) \underline{g}_k \underline{f}_k^* \tag{51}$$

[46,51] $$E_k^f = \lambda E_{k-N}^f + \underline{\xi}_{k+N} \underline{x}_k^* (-\underline{g}_k \underline{f}_k^*) + (\underline{f}_k + F_{k-N}^* \underline{x}_k - V_k^{f*} \underline{g}_k) \underline{f}_k^* + \underline{\xi}_{k+N} \underline{x}_k^* \underline{g}_k \underline{f}_k^* \tag{52}$$

[52] $$E_k^f = \lambda E_{k-N}^f + (\underline{f}_k + F_{k-N}^* \underline{x}_k - V_k^{f*} \underline{g}_k) \underline{f}_k^* \tag{53}$$

[43,46] $$A_k (F_{k-N} + \underline{g}_k \underline{f}_k^*) = V_k^f \tag{54}$$

[54] $$\underline{g}_k \underline{f}_k^* = A_k^{-1} V_k^f - F_{k-N} \tag{55}$$

[19,55] $$\underline{f}_k \underline{g}_k^* \underline{x}_k = V_k^{f*} \underline{g}_k - F_{k-N}^* \underline{x}_k \tag{56}$$

Since $\underline{g}_k^* \underline{x}_k$ is a scalar,

[53,56] $$E_k^f = \lambda E_k^f + (1-\underline{g}_k^* \underline{x}_k) \underline{f}_k \underline{f}_k^* . \tag{57}$$

One more identity is needed for the forward predictor.

[40,56] $$\underline{f}_k = \underline{\xi}_{k+N} + \underline{f}_k \underline{g}_k^* \underline{x}_k - V_k^{f*} \underline{g}_k \tag{58}$$

Define $\underline{f}_k'$ as follows.

$$\underline{f}_k' \triangleq (1-\underline{g}_k^* \underline{x}_k) \underline{f}_k \tag{59}$$

[58,59] $$\underline{f}_k' = \underline{\xi}_{k+N} - V_k^{f*} \underline{g}_k \tag{60}$$

2.6.2 Backward Prediction

Define the vector $\underline{\rho}_k$ composed of the N+1 elements leaving the state vector at the k^{th} sample time (when k/N is an integer) as follows.

$$\underline{\rho}_k^T \triangleq [u_{k-K_1-1} \; u_{k-K_1-2} \cdots u_{k-K_1-N} \; d_{k-D-NK_2-N}] \tag{61}$$

The linear backward prediction of $\underline{\rho}_k$ based upon $\underline{x}_k$ is $B_{k-N}^* \underline{x}_k$ where B_k is an (N+1) x (K_1+1+K_2) dimensional matrix of backward prediction coefficients. The backward prediction error vector is defined as

$$\underline{b}_k \triangleq \underline{\rho}_k - B_{k-N}^* \underline{x}_k , \tag{62}$$

and the backward prediction LS cost function is

$$\text{backward prediction LS cost function} = \sum_{n=0}^{k/N} \lambda^{n-k/N} \, (\underline{\rho}_{nN} - B_k^* \underline{x}_{nN})(\underline{\rho}_{nN} - B_k^* \underline{x}_{nN})^* \, . \tag{63}$$

Denote the optimal value of this cost function as E_k^b and define the following two matrices.

$$V_k^b \triangleq \sum_{n=0}^{k/N} \lambda^{n-k/N} \, \underline{x}_{nN} \, \underline{\rho}_{nN}^* = \lambda \, V_{k-N}^b + \underline{x}_k \, \underline{\rho}_k^* \tag{64}$$

$$R_k^b \triangleq \sum_{n=0}^{k/N} \lambda^{n-k/N} \, \underline{\rho}_{nN} \underline{\rho}_{nN}^* = \lambda \, R_{k-N}^b + \underline{\rho}_k \, \underline{\rho}_k^* \tag{65}$$

The derivation of the backward predictor is identical to that of the forward predictor. Because the definitions given by Equations (61) through (65) are consistent with those of the forward predictor, replacement of the quantities F_k, $\underline{f}_k$, V_k^f, E_k^f, R_k^f, $\underline{\xi}_{k+N}$ and $\underline{f}_k'$, by B_k, $\underline{b}_k$, V_k^b, E_k^f, R_k^b, $\underline{\rho}_k$ and $\underline{b}_k'$, respectively, into Equations (43) through (60) produces the mathematical framework of the backward predictor. The expressions needed for subsequence derivations are stated below.

[43] $$A_k \, B_k = V_k^b \tag{66}$$

[46] $$B_k = B_{k-N} + \underline{g}_k \, \underline{b}_k^* \tag{67}$$

[47] $$E_k^b = R_k^b - V_k^{b*} \, B_k \tag{68}$$

[60] $$\underline{b}_k' \triangleq \underline{\rho}_k - V_k^{b*} \, \underline{g}_k \quad . \tag{69}$$

2.6.3 Extended State DFE Adaptation

From Equations (39) and (61) the elements of $\underline{\xi}_k$ and $\underline{\rho}_k$ are never contained within the same state vector. To establish the interrelationship of E_k^b and V_k^b with E_k^f and V_k^f, an extended DFE is considered. The state vector of this extended DFE is defined below.

$$\underline{\bar{x}}_k^T \triangleq [u_k \; u_{k-1} \; \cdots \; u_{k-K_1-N} \; d_{k-D-N} \; d_{k-D-2N} \; \cdots \; d_{k-D-NK_2-N}] \tag{70}$$

Since this extended DFE is just the original DFE with the parameter K_1 increased by N and the parameter K_2 increased by 1, Equations (8) through (38) apply here directly. Only the following two expressions related to the extended DFE will be needed however.

[11] $$\bar{A}_k \triangleq \sum_{n=0}^{k/N} \lambda^{n-k/N} \, \underline{\bar{x}}_{nN} \, \underline{\bar{x}}_{nN}^* \tag{71}$$

[19] $$\bar{A}_k \, \underline{\bar{g}}_k = \underline{\bar{x}}_k \tag{72}$$

where $\underline{\bar{g}}_k$ is the extended Kalman gain vector.

2.6.4 Derivation of the Algorithm

To relate $\bar{A}_k$ and $\underline{\bar{x}}_k$ to A_k and $\underline{x}_k$, two (K_1+K_2+N+2) dimensional square matrices are introduced.

$$Q_f \triangleq \begin{bmatrix} I_N & & \\ & 1 & \\ & I_{K_1+1} & \\ & & I_{K_2} \end{bmatrix} \qquad Q_b \triangleq \begin{bmatrix} I_{K_1+1} & & \\ & & I_{K_2} \\ & I_N & \\ & & 1 \end{bmatrix}$$

It is easy to verify that Q_f and Q_b have the following properties.

$$Q_f^T = Q_f^{-1} \tag{73}$$

$$Q_b^T = Q_b^{-1} \tag{74}$$

$$Q_f \, \bar{\underline{x}}_k = \begin{bmatrix} \underline{\xi}_k \\ - - - \\ \underline{x}_{k-N} \end{bmatrix} \tag{75}$$

$$Q_b \, \bar{\underline{x}}_k = \begin{bmatrix} \underline{x}_k \\ - - - \\ \underline{\rho}_k \end{bmatrix} \tag{76}$$

Next the extended Kalman gain vector is expressed in terms of the forward predictor variables.

$$[71] \qquad Q_f \, \bar{A}_k \, Q_f^T = \sum_{n=0}^{k/N} \lambda^{n-k/N} \, Q_f \, \bar{\underline{x}}_{nN} \, \bar{\underline{x}}_{nN}^* \, Q_f^T \tag{77}$$

$$[75,77] \qquad Q_f \, \bar{A}_k \, Q_f^T = \sum_{n=0}^{k/N} \lambda^{n-k/N} \begin{bmatrix} \underline{\xi}_{nN} \\ - - - - \\ x_{nN-N} \end{bmatrix} \begin{bmatrix} \underline{\xi}_{nN}^* & \underline{x}_{nN-N}^* \end{bmatrix} \tag{78}$$

$$[11,44,48,78] \qquad Q_f \, \bar{A}_k \, Q_f^T = \begin{bmatrix} R_{k-N}^f & V_{k-N}^{f*} \\ V_{k-N}^f & A_{k-N} \end{bmatrix} \tag{79}$$

$$[72] \qquad Q_f \, \bar{A}_k \, \bar{\underline{g}}_k = Q_f \, \bar{\underline{x}}_k \tag{80}$$

$$[73,75,79,80] \quad -(Q_f \bar{A}_k Q_f^T)\, Q_f\, \bar{g}_k = -\begin{bmatrix} \underline{\xi}_k \\ - - - \\ \underline{x}_{k-N} \end{bmatrix} \tag{81}$$

$$[19,79] \quad Q_f \bar{A}_k\, Q_f^T \begin{bmatrix} \underline{0} \\ - - - \\ \underline{g}_{k-N} \end{bmatrix} = \begin{bmatrix} V_{k-N}^{f*}\, \underline{g}_{k-N} \\ - - - - - - \\ \underline{x}_{k-N} \end{bmatrix} \tag{82}$$

$$[43,47,79] \quad Q_f\, \bar{A}_k\, Q_f^T \begin{bmatrix} I \\ - - - \\ -F_{k-N} \end{bmatrix} = \begin{bmatrix} R_{k-N} - V_{k-N}^{f*} F_{k-N} \\ - - - - - - - - \\ \underline{0} \end{bmatrix} = \begin{bmatrix} E_{k-N}^f \\ - - - \\ \underline{0} \end{bmatrix} \tag{83}$$

By Equation (59) the left side of Equation (83) can be postmultiplied by $(E_{k-N}^f)^{-1}\, \underline{f}'_{k-N}$ while the right side is postmultiplied by $(E_{k-N}^f)^{-1}(\underline{\xi}_k - V_{k-N}^{f*} \underline{g}_{k-N})$.

$$[83,59] \quad Q_f\, \bar{A}_k\, Q_f^T \begin{bmatrix} (E_{k-N}^f)^{-1} \underline{f}'_{k-N} \\ - - - - - - - - - - \\ -F_{k-N}(E_{k-N}^f)^{-1} \underline{f}'_{k-N} \end{bmatrix} = \begin{bmatrix} \underline{\xi}_k - V_{k-N}^{f*} \underline{g}_{k-N} \\ - - - - - - - \\ \underline{0} \end{bmatrix} \tag{84}$$

By inspection the right sides of equations (81), (82) and (84) sum to zero. Setting the sum of the left sides to zero and premultiplying by the inverse of $Q_f\, \bar{A}_k\, Q_f^T$ yields

$$[81,82,84] \quad Q_f\, \bar{g}_k = \begin{bmatrix} (E_{k-N}^f)^{-1} \underline{f}'_{k-N} \\ - - - - - - - - - - - - \\ \underline{g}_{k-N} - F_{k-N}(E_{k-N}^f)^{-1} \underline{f}'_{k-N} \end{bmatrix} \tag{85}$$

A similar derivation is now performed to express the extended Kalman gain vector in terms of the backward predictor variables.

$$[71] \qquad Q_b \bar{A}_k Q_b^T = \sum_{n=0}^{k-N} \lambda^{n-k/N} Q_b \bar{\underline{x}}_{nN} \underline{x}^*_{nN} Q_b^T \tag{86}$$

$$[86,76] \qquad Q_b \bar{A}_k Q_b^T = \sum_{n=0}^{k/N} \lambda^{n-k/N} \begin{bmatrix} \underline{x}_{nN} \\ - - - \\ \underline{\rho}_{nN} \end{bmatrix} \begin{bmatrix} \underline{x}^*_{nN} & \underline{\rho}^*_{nN} \end{bmatrix} \tag{87}$$

$$[11,65,66,87] \qquad Q_b \bar{A}_k Q_b^T = \begin{bmatrix} A_k & V_k^b \\ V_k^{b*} & R_k^b \end{bmatrix} \tag{88}$$

$$[72] \qquad Q_b \bar{A}_k \bar{\underline{g}}_k = Q_b \bar{\underline{x}}_k \tag{89}$$

$$[74,76,88,89] \qquad (Q_b \bar{A}_k Q_b^T) Q_b \bar{\underline{g}}_k = \begin{bmatrix} \underline{x}_k \\ - - - - \\ V_k^{b*} \underline{g}_k \end{bmatrix} \tag{90}$$

$$[19,88] \qquad Q_b \bar{A}_k Q_b^T \begin{bmatrix} \underline{g}_k \\ - - \\ \underline{0} \end{bmatrix} = \begin{bmatrix} \underline{x}_k \\ - - - - \\ V_k^{b*} \underline{g}_k \end{bmatrix} \tag{91}$$

$$[66,68,88] \qquad Q_b \bar{A}_k Q_b^T \begin{bmatrix} -B_k \\ - - - \\ I \end{bmatrix} = \begin{bmatrix} 0 \\ - - - - - \\ R_k^b - V_k^{b*} B_k \end{bmatrix} = \begin{bmatrix} 0 \\ - - \\ E_k^b \end{bmatrix} \tag{92}$$

$$[69,92] \quad Q_b \bar{A}_k Q_b^T \begin{bmatrix} -B_k (E_k^b)^{-1} \underline{b}_k' \\ \hline (E_k^b)^{-1} \underline{b}_k' \end{bmatrix} = \begin{bmatrix} \underline{0} \\ \hline \underline{\rho}_k - V_k^{b*} \underline{g}_k \end{bmatrix} \tag{93}$$

$$[90,91,93] \quad Q_b \bar{\underline{g}}_k = \begin{bmatrix} \underline{g}_k - B_k (E_k^b)^{-1} \underline{b}_k' \\ \hline (E_k^b)^{-1} \underline{b}_k' \end{bmatrix} \tag{94}$$

Define a K_1+1+K_2 column vector $\underline{g}_k'$ and an $N+1$ length column vector $\underline{\mu}_k$ as

$$\begin{bmatrix} \underline{g}_k' \\ \hline \underline{\mu}_k \end{bmatrix} \triangleq Q_b \bar{\underline{g}}_k \tag{95}$$

Notice that $\underline{g}_k'$ and $\underline{\mu}_k$ can be generated by rearranging the elements of the partitioned column vector shown on the right side of Equation (85). A comparison of Equations (94) and (95) leads to the following expression.

$$[94,95] \quad \underline{g}_k = \underline{g}_k' + B_k \underline{\mu}_k \tag{96}$$

A recursive expression for B_k using $\underline{g}_k'$, $\underline{\mu}_k$ and $\underline{b}_k$ can now be derived.

$$[67,96] \quad B_k = B_{k-N} + (\underline{g}_k' + B_k \underline{\mu}_k) \underline{b}_k^* \tag{97}$$

[97] $$B_k(I - \underline{\mu}_k \underline{b}_k^*) = B_{k-N} + \underline{g}_k' \underline{b}_k^* \qquad (98)$$

We assume $I - \underline{\mu}_k \underline{b}_k^*$ is invertible.

[98] $$B_k = (B_{k-N} + \underline{g}_k' \underline{b}_k^*)(I - \underline{\mu}_k \underline{b}_k^*)^{-1} \qquad (99)$$

The sequence of operations performed by this algorithm after the k^{th} sample time (when k/N is an integer) is

[40] $$f_{k-N} = \underline{\xi}_k - F_{k-2N}^* \underline{x}_{k-N}$$

[46] $$F_{k-N} = F_{k-2N} + \underline{g}_{k-N} \underline{f}_{k-N}^*$$

[59] $$\underline{f}_{k-N}' = (1 - \underline{g}_{k-N}^* \underline{x}_{k-N}) \underline{f}_{k-N}$$

[57,59] $$E_{k-N}^f = \lambda E_{k-2N}^f + \underline{f}_{k-N}' \underline{f}_{k-N}^*$$

[85,94] $$\begin{bmatrix} -\underline{g}_k' \\ \underline{\mu}_k \end{bmatrix} = Q_b Q_f^T \begin{bmatrix} (E_{k-N}^f)^{-1} \underline{f}_{k-N}' \\ \hline \underline{g}_{k-N} - F_{k-N}(E_{k-N}^f)^{-1} \underline{f}_{k-N}' \end{bmatrix}$$

[62] $$\underline{b}_k = \underline{\rho}_k - B_{k-N}^* \underline{x}_k$$

[99] $$B_k = (B_{k-N} + \underline{g}_k' \underline{b}_k^*)(I - \underline{\mu}_k \underline{b}_k^*)^{-1}$$

[96] $$g_k = g'_k + B_k \mu_k$$

[21] $$\varepsilon_k = d_{k-D} - \underline{c}^*_{k-N} \underline{x}_k$$

[23] $$\underline{c}_k = \underline{c}_{k-N} + \underline{g}_k \varepsilon^*_k$$

The operation of a T/N fractionally-spaced DFE using the fast Kalman adaptation algorithm is shown in Algorithm 2. Experience has shown that the direct implementation of algorithms such as this can exhibit numerical instability. Often adherence to the IEEE floating point standard results in a stable implementation. Alternately, the algorithm can be restructured in the form of the so-called square root filter to improve numerical stability.

Algorithm No. 2. An adpative T/2-spaced DFE (fast Kalman algorithm).

Step Number	Operation	Comment
1	$k \leftarrow 0$ $\underline{g}_{k-N} \leftarrow \underline{x}_{k-N} \leftarrow \underline{0}$ $F_{k-2N} \leftarrow B_{k-N} \leftarrow 0$ $E_{k-2N} \leftarrow \delta I$ (δ a small positive real number)	Initialization
2	$\underline{f}_{k-N} \leftarrow \underline{\varepsilon}_k - F^*_{k-2N}\,\underline{x}_{k-N}$	Forward predictor error
3	$F_{k-N} \leftarrow F_{k-2N} + \underline{g}_{k-N}\,\underline{f}^*_{k-N}$	Forward predictor
4	$\underline{f}'_{k-N} \leftarrow (1 - \underline{g}^*_{k-N}\underline{x}_{k-N})\,\underline{f}_{k-N}$	$\underline{g}^*_{k-N}\,\underline{x}_{k-N}$ is a real scalar
5	$E^f_{k-N} = \lambda\, E^f_{k-2N} + \underline{f}'_{k-N}\,\underline{f}^*_{k-N}$	E^f_k is hermitian
6	$\begin{bmatrix} \underline{g}'_k \\ - - \\ \underline{u}_k \end{bmatrix} + Q_b\, Q_f^T \begin{bmatrix} (E^f_{k-N})^{-1}\underline{f}'_{k-N} \\ - - - - - - - - - - - - \\ \underline{g}_{k-N} - F_{k-N}(E^f_{k-N})^{-1}\underline{f}_{k-N} \end{bmatrix}$	Multiplication by $Q_b\, Q_f^T$ merely records column vector
7	$\underline{x}_k \leftarrow S\,\underline{x}_{k-N} + P \begin{bmatrix} u_k \\ u_{k-1} \\ \cdot \\ \cdot \\ \cdot \\ u_{k-N+1} \end{bmatrix} + \underline{a}\, d_{k-D-N}$	Shift N new channel samples and previous decision sample into state vector
8	$\underline{b}_k \leftarrow (B_{k-N} + \underline{g}'_k \underline{b}^*_k)(I - \underline{u}_k \underline{b}^*_k)^{-1}$	Backward predictor error
9	$B_k \leftarrow (B_{k-N} + \underline{g}'_k \underline{b}^*_k)(I - \underline{u}_k \underline{b}^*_k)^{-1}$	Backward predictor coefficients
10	$\underline{g}_k \leftarrow \underline{g}'_k + B_k\,\underline{u}_k$	Kalman gain vector
11	$y_k \leftarrow \underline{c}^*_{k-N}\,\underline{x}_k$	Equalization
12	$\epsilon_k \leftarrow d_{k-D} - y_k$	Equalizer error
13	$\underline{c}_k \leftarrow \underline{c}_{k-N} + \underline{g}_k\,\epsilon^*_k$	Update equalizer coefficients
14	$k \leftarrow k + N$	Transition to next set of N input samples
15	go to Step 2	

SECTION 3
SIMULATION DESCRIPTION

This section describes the Monte Carlo computer simulation used to evaluate the adaptive equalizer algorithms discussed in the previous section. The simulation is partitioned into four components as shown in Figure 3. This simulation structure intentionally resembles the signal flow diagram of a one-way HF link. The transmitted waveform is first synthesized into a sampled-data representation, then corrupted by the propagation medium, and finally processed within the receiver. The transmitted and received digital data streams are compared to accumulate a symbol error rate statistic. Each of the four components shown in Figure 3 are described in this section.

3.1 TRANSMITTED SIGNAL GENERATOR

This component of the computer simulation generates the sample sequence $\{d_k\}$ discussed in Section 2.1. The scope of this report is limited to binary PSK modulation, so all channel samples are binary. Further the information bearing symbols (also referred to as bits) are assumed to be random, independent and uncorrelated. A pseudo-random number generator implemented in software generates a stream of random ones and zeroes constituting the information symbols.

Recall from Section 2 that N identical and consecutive samples are generated for each channel symbol, and that k is the sample, not symbol, index. Also recall that for BPSK modulation the elements of

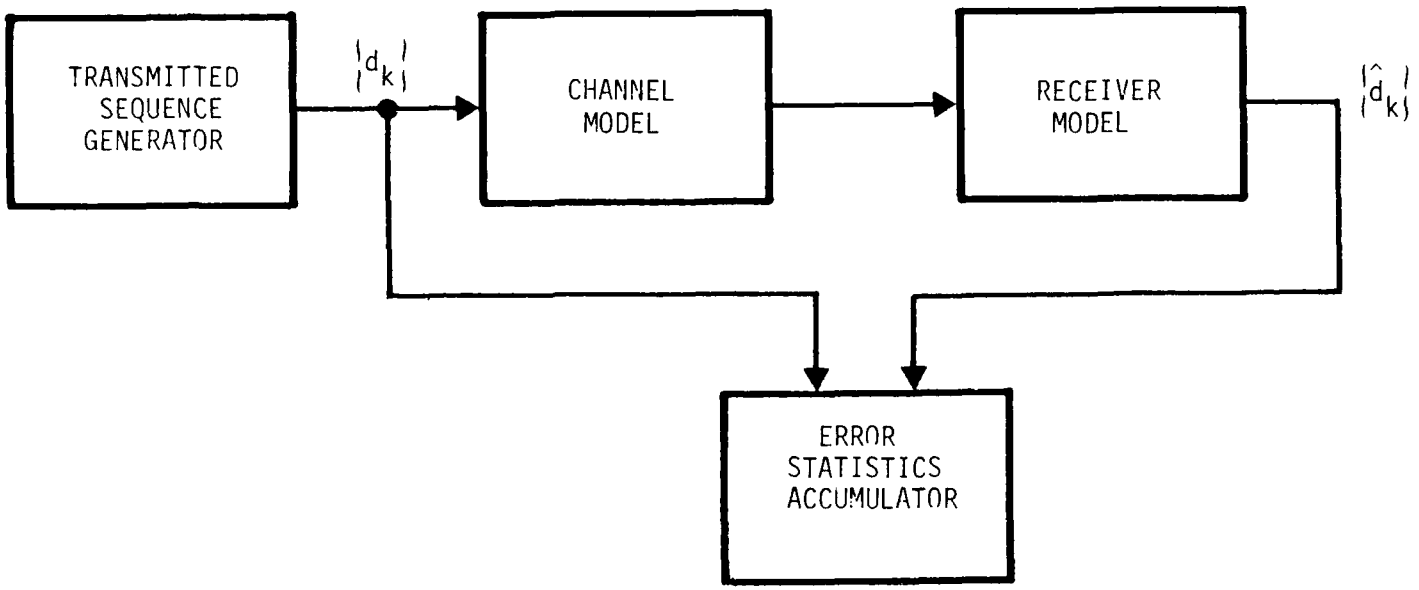

Figure 3. Block diagram of digital PSK HF link simulation.

The BPSK receiver that does employ adaptive equalization is Receiver Model No. 2, described in Section 3.3.2. The equalizer parameters used here are the following:

$$L_{TS} = 42$$

$$L_{TB} = 640$$

$$N = 2$$

$$K_1 = 20$$

$$K_2 = 10$$

$$\Delta = \begin{cases} 1 \times 10^{-3} & \text{after reception of an information symbol} \\ 4 \times 10^{-3} & \text{after reception of a training symbol} \end{cases}$$

The two simulated links were exercised for E_s/N_o equal to 6 and 10 dB. The signal-to-noise ratio for the DFE-assisted modem was actually reduced by 0.2948 dB to allow for the seven percent training sequence overhead. Thus the two modem types are compared on the basis of equal transmitted energy per information symbol.

Where E_{ISI} diminishes, that is E_{ISI}/E_s is $-\infty$ dB, the average bit error rate for Receiver Model No. 1 is given by

$$P_e = \frac{1}{2} \text{Erfc} \left(\sqrt{E_s/N_o}\right)$$

where Erfc(•) is the familiar complementary error function. Evaluation of this expression for E_s/N_o equaling 6 and 10 dB yields 2.388×10^{-3} and 3.8756×10^{-6}, respectively.

The average bit error rate for Receiver Model No. 1 with E_s equaling 6 dB is plotted versus E_{ISI}/E_s in Figure 9. As E_{ISI} diminishes the curve appears to approach the predicted value of 2.388×10^{-3}. The

SECTION 4
RESULTS AND CONCLUSIONS

This section presents two sets of results that were generated during this investigation. The first set is a comparison of the performance of an idealized conventional BPSK receiver to that of a DFE-assisted BPSK receiver in the context of the time-invariant, frequency-selective channel model described in Section 3.2.1. These results are presented to illustrate the problem of intersymbol interference and show that adaptive equalization is a potential mitigation technique.

The second set of results show the DFE-assisted modem performance in the context of the time-varying, frequency-selective channel model discussed in Section 3.2.2. These results give an indication of how this modem type would perform over a range of doppler and delay spreads exhibited by disturbed HF propagation paths.

4.1 PERFORMANCE OF RECEIVER MODELS NO. 1 AND NO. 2 IN THE CONTEXT OF CHANNEL MODEL NO. 1.

The Monte Carlo computer simulation was exercised to investigate the performance of the two BPSK modems described in Section 3.3 operating under the time-invariant, frequency-selective channel conditions discussed in Section 3.2.1.

The BPSK receiver not employing adaptive equalization is Receiver Model No. 1, described in Section 3.3.1. It does not use a training sequence and is bit synchronized and phase locked onto the signal energy propagation mode.

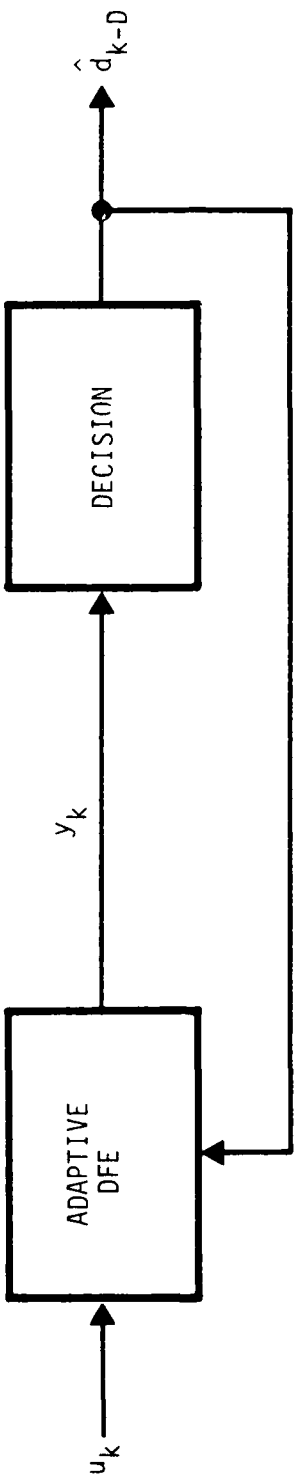

Figure 8. Block diagram of Receiver Model No. 2.

the simulation. Instead the decision rule offset delay parameter D is selected so that all signal energy associated with d_{k-D} is in the feed forward section of the DFE when y_k is generated.

A block diagram of the model is shown in Figure 8. It differs from Receiver Model No. 1 in three ways: 1) a DFE has replaced the N-sample accumulation function; 2) the parameter D is larger than zero; and 3) the decision symbol $\hat{d}_{k-D}$ is fed back to the DFE function.

DFE adaptation can be implemented using either Algorithm 1 of Section 2.3 or Algorithm 2 of Section 2.6, with one modification. The variable d_{k-D} of Step 4 of Algorithm 1 and Step 12 of Algorithm 2 must be replaced by $\hat{d}_{k-D}$. The decision rule for $\hat{d}_{k-D}$ for Receiver Model No. 1 differs from Receiver Model No. 2 because of the incorporation of training sequence symbols into the telemetry format. The rule is given by:

$$\hat{d}_{k-D} = \begin{cases} +1 & \text{Real } \{y_k\} \geq 0 \text{ and } d_{k-D} \text{ was generated from an information symbol} \\ -1 & \text{Real } \{y_k\} < 0 \text{ and } d_{k-D} \text{ was generated from an information symbol} \\ d_{k-D} & d_{k-D} \text{ was generated from a training symbol} \end{cases}$$

3.4 ERROR STATISTICS ACCUMULATION

This part of the simulation simply compares the sequence $\{\hat{d}_k\}$ with $\{d_k\}$ to form an estimate of the average symbol error rate. The error rate estimate is calculated by dividing the number of incorrectly received information symbols by the total number of received information symbols. Training sequence symbols are only used to adapt the DFE and are not used in the calculation of the error rate estimate.

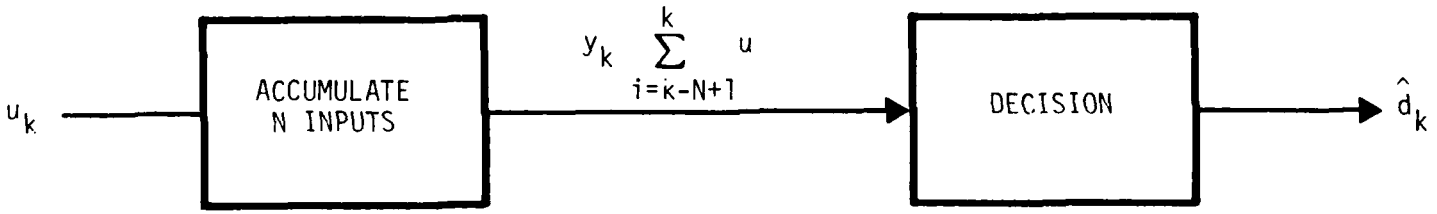

Figure 7. Block diagram of Receiver Model No. 1.

3.3.1 Receiver Model No. 1: An Idealized Conventional BPSK Receiver Model

This receiver model is only considered in the context of the simply delay spread channel model described in Section 3.2.1. The receiver is assumed to be synchronized and phase-locked onto the mode propagating signal energy. Since the signal energy mode is represented by h_k^0, the decision variable sequence is denoted $\{\hat{d}_k\}$. The delay parameter D equals zero because $\hat{d}_k$ can be generated immediately after the k^{th} sampling interval.

This receiver model is represented by Figure 7. A value for y_k is generated (for each k that is an integer multiple of N) by simply adding u_k, u_{k-1}, ..., u_{k-N+1}. The binary decision variable $\hat{d}_k$ is then formed by the following rule:

$$\hat{d}_k = \begin{cases} 1 & \text{Real } \{y_k\} \geq 0 \\ -1 & \text{Real } \{y_k\} < 0 \end{cases}$$

where again $\hat{d}_k$ is only calculated when k is an integer multiple of N. By definition, the channel input samples d_k, d_{k-1}, ..., d_{k-N+1} are equal, being identically generated from the same channel input symbol as discussed in Section 3.1.

3.3.2 Receiver Model No.2: A DFE-Assisted BPSK Receiver

This receiver model is used for both channel models discussed in Section 3.2. The DFE explicitly provides the phase tracking and "fine" bit synchronization functions that are assumed to be perfect in Receiver Model No. 1. In an operational receiver a "coarse" bit synchronization capability would be required, but this is not implemented explicitly in

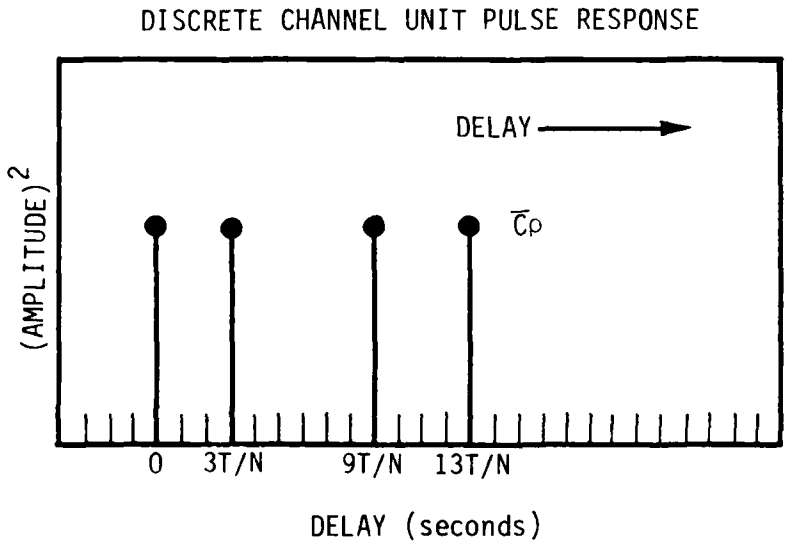

Figure 6. Delay power spectrum of Channel Model No. 2.

B = Doppler bandwidth (hertz)

$\overline{C}$ = average carrier power (watts)

ρ = constant selected so that $\overline{C} = E\{h_k^T d_k\}$ (note that ρ equals 1/2 for N less than four)

For the purposes of this report, this channel model will be specified by the four parameters $\overline{C}/N_o$, B, N and T. $\overline{C}$ is arbitrarily chosen to be unity without loss of generality. Since the parameter $\overline{C}/N_o$ has units of watts/joule or hertz rather than being a unitless ratio, the logarithmic form of the $\overline{C}/N_o$ specification has units of dB-Hz (decibels relative to a one hertz bandwidth). The delay spectrum for the channel model is illustrated by Figure 6.

This channel model shall not be employed to investigate conventional BPSK modems, such as Receiver Model No. 1, which can only lock onto one of the four modes. Therefore it is not appropriate to designate one mode as the propagation path for signal energy with which all other modes interfere. Rather the received energy from each mode of Channel Model No. 2 is considered signal energy even though the four modes interfere destructively with one another on the average.

3.3 RECEIVER MODELS

A receiver model generates the decision variable sequence $\{\hat{d}_{k-D}\}$ (for all k that are integer multiples of N) by processing the channel model output symbol sequence $\{u_k\}$.

Two receiver models have been employed for this investigation - one that models an idealized conventional BPSK receiver and another that models an adaptive DFE assisted receiver.

model is inadequate if the modes exhibit different doppler frequency shifts. Such channels are said to have a doppler spread and can be represented by a channel model that allows a distinct phase rotation rate for each mode. One such channel model is described below.

3.3.2 Channel Model No. 2: A Simple Delay and Doppler Spread Model

This model can also be represented using the notation of Section 2.

$$L = 13$$

$$h_k^m = \begin{cases} \sqrt{\bar{C}\rho}\ \exp\{0.375 \cdot 2\pi kBT/N\} & \text{for } m = 0 \\ \sqrt{\bar{C}\rho}\ \exp\{0.125 \cdot 2\pi kBT/N\} & \text{for } m = 3 \\ \sqrt{\bar{C}\rho}\ \exp\{0.250 \cdot 2\pi kBT/N\} & \text{for } m = 9 \\ \sqrt{\bar{C}\rho}\ \exp\{0.625 \cdot 2\pi kBT/N\} & \text{for } m = 13 \\ 0 & \text{otherwise} \end{cases}$$

$$E\{n_k n_j^k\} = \begin{cases} N_o N/T & k = j \\ 0 & k \neq j \end{cases}$$

where k, N, n_k, N_o retain the same definitions as in Section 3.3.1 and

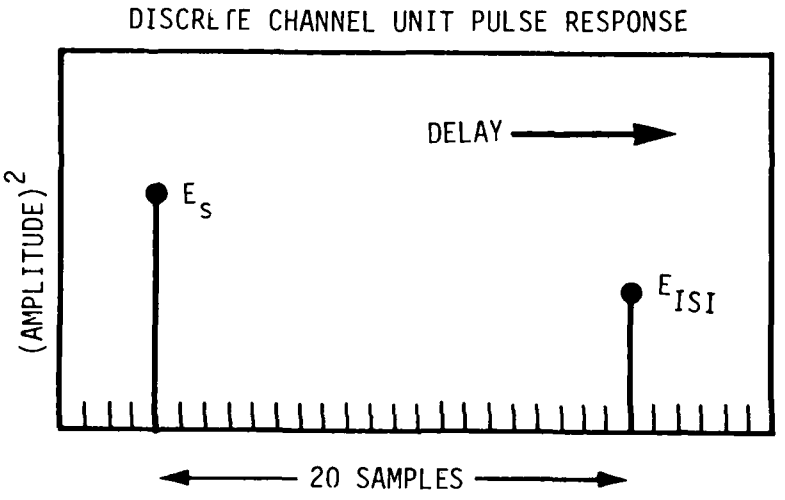

Figure 5. Delay power spectrum of Channel Model No. 1.

N = ratio of sampling rate to modulation rate

n_k = complex zero-mean, additive white Gaussian component of Equation 2 of Section 2. Here the quadrature real and imaginary components of n_k are uncorrelated and have the same variance

N_o = one-side power spectral density level of each quadrature component of the additive white noise preceding sampler.

For the purposes of this report, this channel model will be specified by the three parameters E_s/N_o, E_s/E_{ISI} and N. E_s and T are arbitrarily chosen to be unity without loss of generality.

This channel model can be visualized using Figure 5 which shows a two mode energy delay spectrum resulting from the transmission of an impulse. The earliest (left most) spike corresponds to the mode propagating signal energy and the other spike corresponds to the mode propagating intersymbol interference energy. The association of one mode with the signal and the other with the intersymbol interference is motivated by how this channel model might affect a conventional PSK receiver. Assuming the delay between the two modes exceeds a channel symbol interval (i.e., N is less than 20) the matched filter of a conventional PSK demodulor cannot combine energy from both modes that arises from the same channel symbol.

This channel model approximates only a limited range of HF propagation possibilities. Three examples might be simultaneous reception from: 1) a groundwave and a skywave propagation path; 2) a single hop and a double hop path; and 3) two single hop paths reflecting off distinct ionospheric layers. In the context of adaptive equalization, the above

effects. Reference 16 reviews the current state of the art in HF propagation analysis in the context of nuclear phenomenology.

Since the current understanding of HF propagation disturbances is incomplete, the choice of a channel model is somewhat arbitrary. Here two simple, non-statistical channel models shall be employed, which have the salient characteristics needed for this investigation, but are not general representations of HF channels. The first is time invariant, exhibiting delay spread but not doppler spread. The second exhibits both delay and doppler spreads.

3.2.1 Channel Model No. 1: A Simple Delay Spread Model

Using the notation of Section 2, this channel model can be described by the following set of parameter values.

$$L = 20$$

$$h_k^m = \begin{cases} \sqrt{E_s/T} & m = 0 \\ \sqrt{E_{ISI}/T} & m = 20 \\ 0 & \text{otherwise} \end{cases} \qquad \text{for all } k$$

$$E\{n_k n_j^*\} = \begin{cases} N_o N/T & k = j \\ 0 & k \neq j \end{cases}$$

where

k = sample index

E_s = received signal energy per modulation interval

E_{ISI} = received intersymbol interference energy per modulation interval

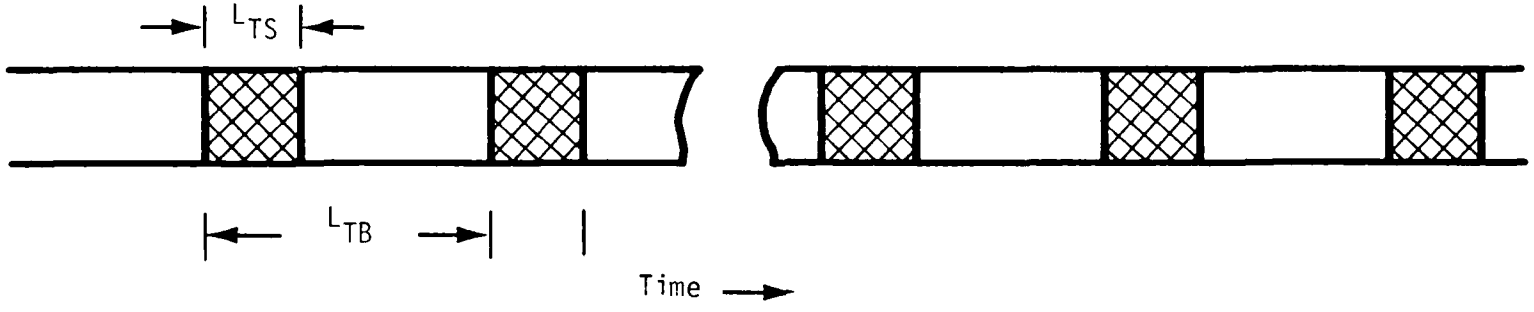

Figure 4a. Representation of telemetry format.

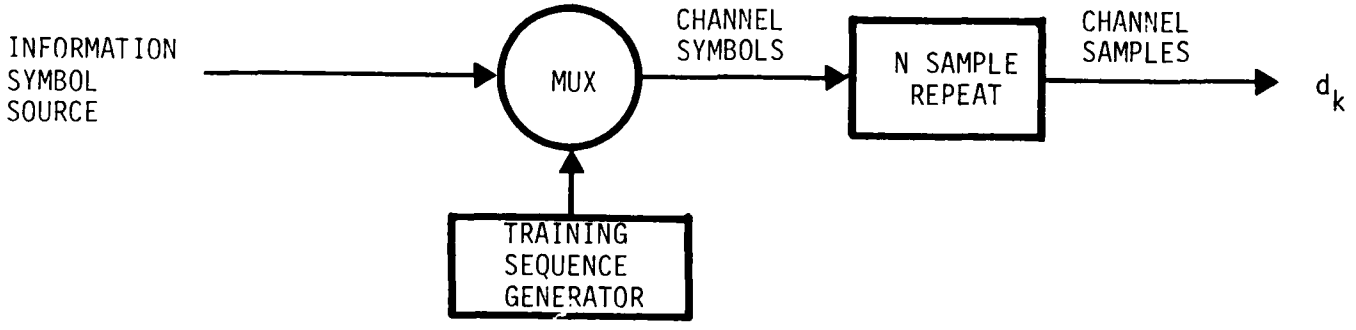

Figure 4b. Signal flow diagram illustrating the generation of the channel sample sequence $\{d_k\}$.

$\{d_k\}$ can be taken from the set $\{1,-1\}$. The convention used in the simulation is as follows: the binary channel symbol 0 is mapped into N consequetive elements of $\{d_k\}$ having the value +1; and channel symbol 1 is similarly mapped into N consecutive elements having the value -1.

In addition to the correspondence with information symbols, some elements of $\{d_k\}$ may correspond to training sequence symbols. A training sequence is a block of channel symbols, known a priori to the receiver, which are periodically injected into the transmitted data stream. Training sequence symbols are used within the receiver to initialize and maintain the adaptation algorithm of the equalizer, as will be discussed in Section 3.3.

The telemetry format of the simulated HF link is shown in Figure 4a. The symbol stream is partitioned into telemetry blocks of L_{TB} symbols in duration. Each telemetry block starts with the same sequence of L_{TS} training symbols (represented by cross-hatching in the figure), followed by a L_{TB}-L_{TS} length segment from the information symbol stream. The multiplexing of the training sequences into the data stream is represented by Figure 4b. The generated sequence $\{d_k\}$ is taken as input by the channel models.

3.2 CHANNEL MODELS

Much experimental and analytic work has been done to characterize HF channels (e.g., References 7-15), but universally accepted models of HF propagation disturbances have yet to be developed. In natural environments, a wide range of channel characteristics, such as absorption, delay spread and doppler spread, have been observed and the most severe effects tend to occur on auroral propagation paths. An important class of artificially induced effects are those resulting from high altitude nuclear bursts. Such effects are not presently well understood, but are estimated to be at least as severe as naturally occurring auroral

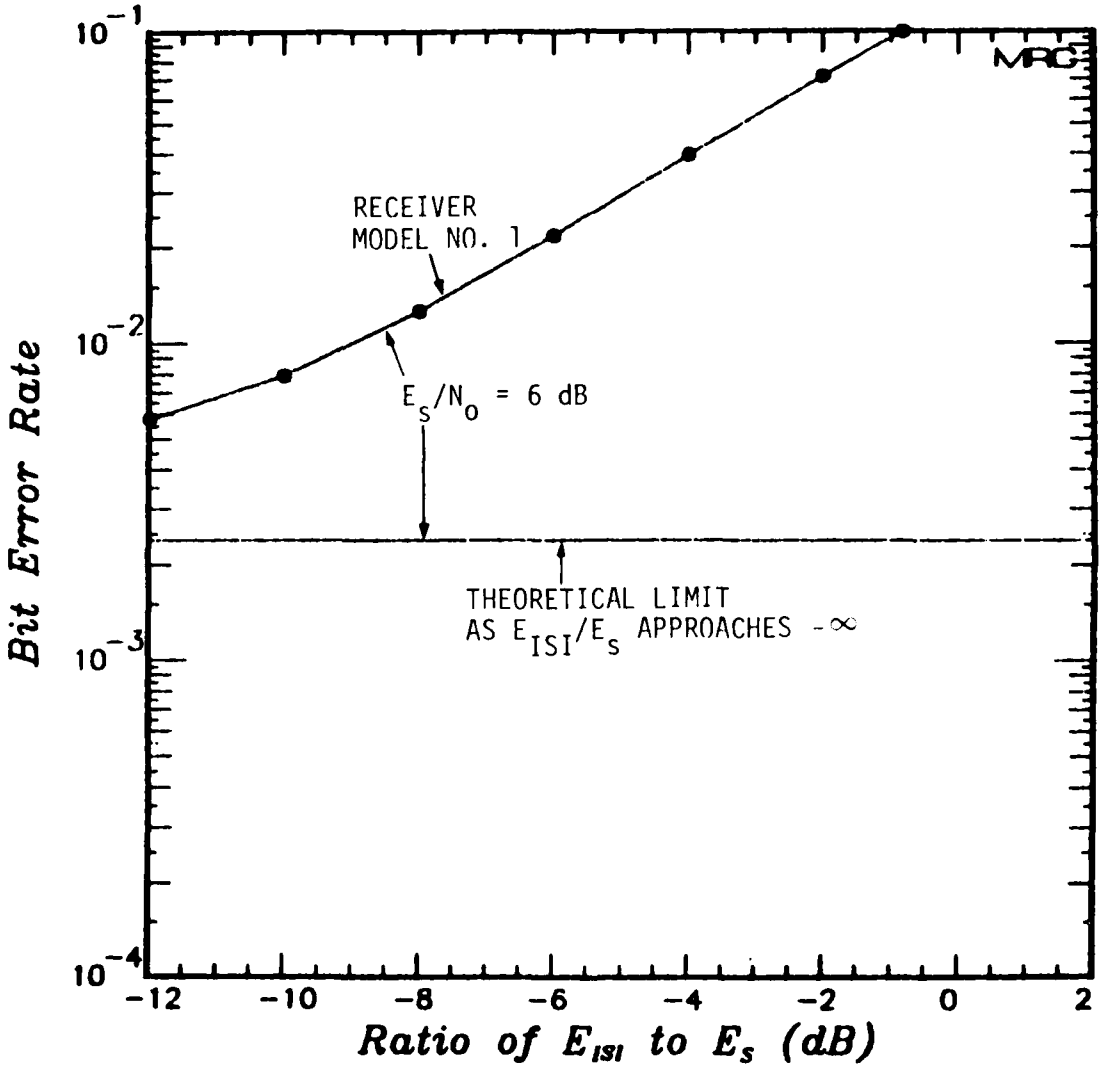

Figure 9. Bit error rate versus E_{ISI}/E_S for Receiver Model No. 1 with E_S/N_O equal to 6 dB.

bit error rate increases with the level of intersymbol interfere as would be expected. The severity with which this error rate increases accounts for the rarity with which this modem type is employed in HF communication links.

Two approaches for improvi g the average bit error rate were explored: increasing the signal-to-noise ratio; and substituting Receiver Model No. 2 for Receiver Model No. 1. Figure 10 presents a comparison of the results of these approaches with the results of Figure 9.

Consider first the difference in error rate characteristics when E_S/N_O is increased from 6 dB to 10 dB. As previously mentioned, this would result in a decrease in average bit error rate from 2.388×10^{-3} to 3.8756×10^{-6} for E_{ISI} equal to zero. Figure 10 shows, though, that as E_{ISI}/E_S is increased, the 10 dB error rate characteristic rapidly approaches the same degraded performance level experienced for 6 dB. Apparently as E_{ISI}/E_S is increased, the significance of the additive white Gaussian noise on the error mechanism diminishes in comparison to the significance of intersymbol interference. Therefore increasing the transmitted carrier power, which increases both E_{ISI} and E_S but leaves E_{ISI}/E_S unaltered, does not effectively combat the effects of high levels of intersymbol interference.

Now consider the difference in error rates with E_S/N_O held at 6 dB when Receiver Model No. 1 is replaced with Receiver Model No. 2 and the attendant change in telemetry format to accommodate a training sequence. When E_{ISI}/E_S is very small, Receiver No. 2 suffers an effective 0.4 dB loss relative to the asymptotic error rate exhibited by Receiver No. 1, but as E_{ISI}/E_S increases the error rate for Receiver No. 2 decreases, rather than increases. The 0.4 dB loss in the absence of intersymbol interference is due in part to the 0.2948 dB training sequence overhead mentioned earlier, and in part to the random misadjustment of the

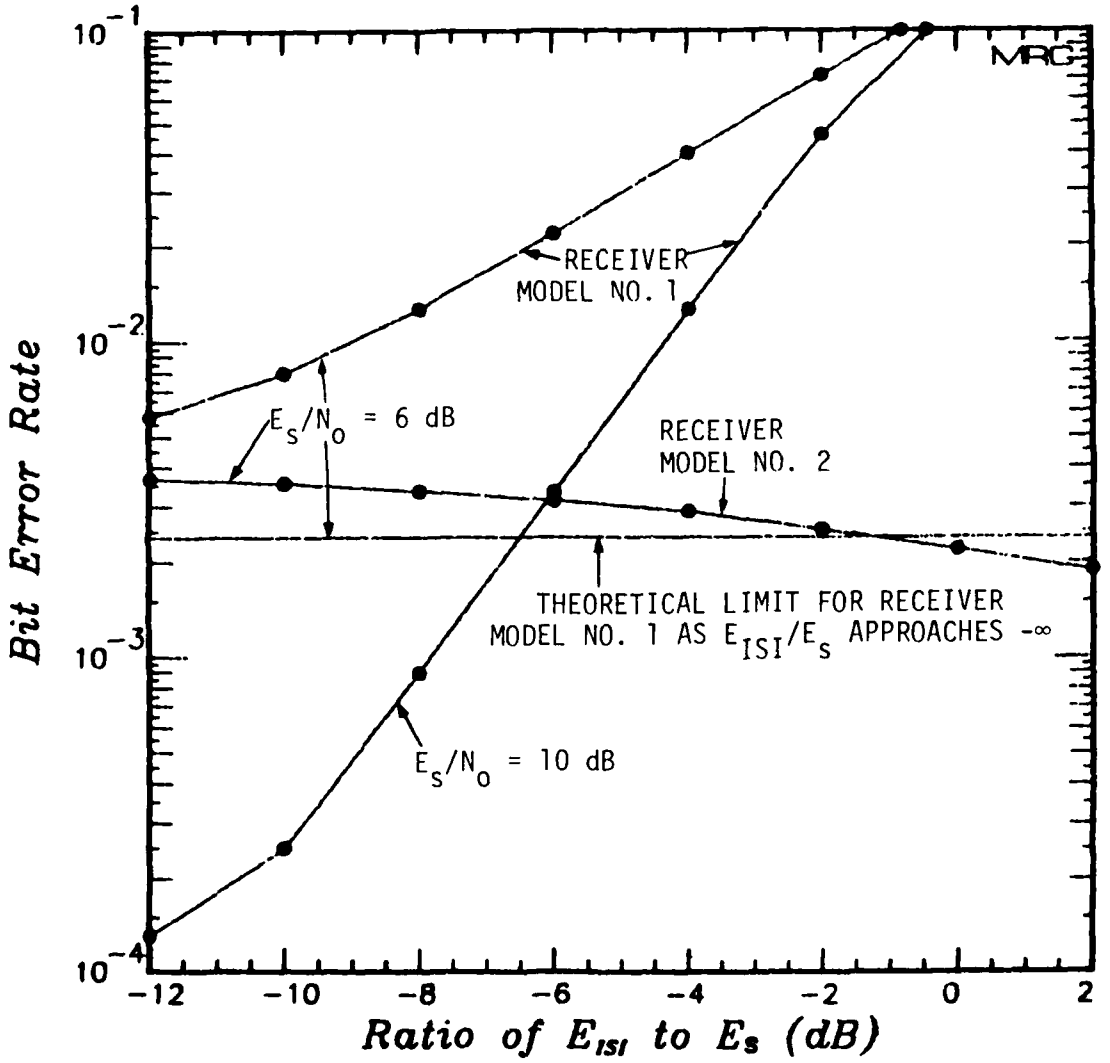

Figure 10. Bit error rate versus E_{ISI}/E_S for both receiver models with E_S/N_O equal to 6 dB and 10 dB.

DFE coefficients caused by the influence of additive white Gaussian noise on the adaptation algorithm. The decrease in average bit error rate with increasing E_{ISI}/E_s results from the DFE using the intersymbol interference energy as additional signal energy.

4.2 PERFORMANCE OF RECEIVER MODEL NO. 2 IN THE CONTEXT OF CHANNEL MODEL NO. 2.

The Monte Carlo simulation was exercised to investigate the performance of the DFE-assisted BPSK modem described in Section 3.3.2 under the time and frequency selective channel conditions discussed in Section 3.2.1. Channel Model No. 1 is time-invariant, allowing the presentation of the results in Section 4.1 to be in a form that is independent of the data rate.

Here Channel Model No. 2 is time-varying, and it is convenient to consider one specific information symbol rate, which was arbitrarily chosen to be 2400 baud. The DFE parameters used to generate all the results presented in the section are as follows:

$$L_{TS} = 48$$

$$L_{TB} = 96$$

$$N = 2$$

$$K_1 = 8$$

$$K_2 = 16$$

$$\Delta = \begin{cases} 2 \times 10^{-3} & \text{after reception of an information symbol} \\ 8 \times 10^{-3} & \text{after reception of a training symbol} \end{cases}$$

$$T = 1/4800 \text{ seconds}$$

Receiver Model No. 1 is not considered here because it does not have a phase tracking capability. The investigation of Receiver Model No. 1 in the context of any time-varying channel model would be pointless.

The stochastic gradient algorithm discussed in Section 2.3 was used within Receiver Model No. 2 to adapt the DFE coefficients. This algorithm has an inherent phase tracking capability which is similar to that of a first order phase lock loop. Since each mode has a fixed doppler offset, the adaptation algorithm must track a phase ramp. This results in a lag error for each DFE coefficient, and the adaptation algorithm could have been redesigned as a second order phase tracking loop to reduce these lag errors. However, by not specifically optimizing the receiver for Channel Model No. 2, the results obtained here are indicative of the performance of this modem type for other channels of comparable doppler spread but exhibiting more random phase fluctuations.

The results take the form of average bit error rates plotted versus either the average carrier power-to-noise spectral density level $\overline{C}/N_0$ of the doppler bandwidth B.

Figure 11 shows the bit error rate versus $\overline{C}/N_0$ for B fixed at four hertz. As expected, the error rate decreases monotonically with increasing $\overline{C}/N_0$. However, the error rate characteristic flattens for values of $\overline{C}/N_0$ above 46 dB-Hz. When $C/\overline{N}_0$ is below this value most detected bit errors are caused by the AWGN component of the channel model output. As $\overline{C}/N_0$ is increased the AWGN component diminishes in comparison to the residual intersymbol interference which the adaptive DFE does not correct. Further increasing $\overline{C}/N_0$ does not appreciably improve the error rate because the effects of intersymbol interference are not reduced.

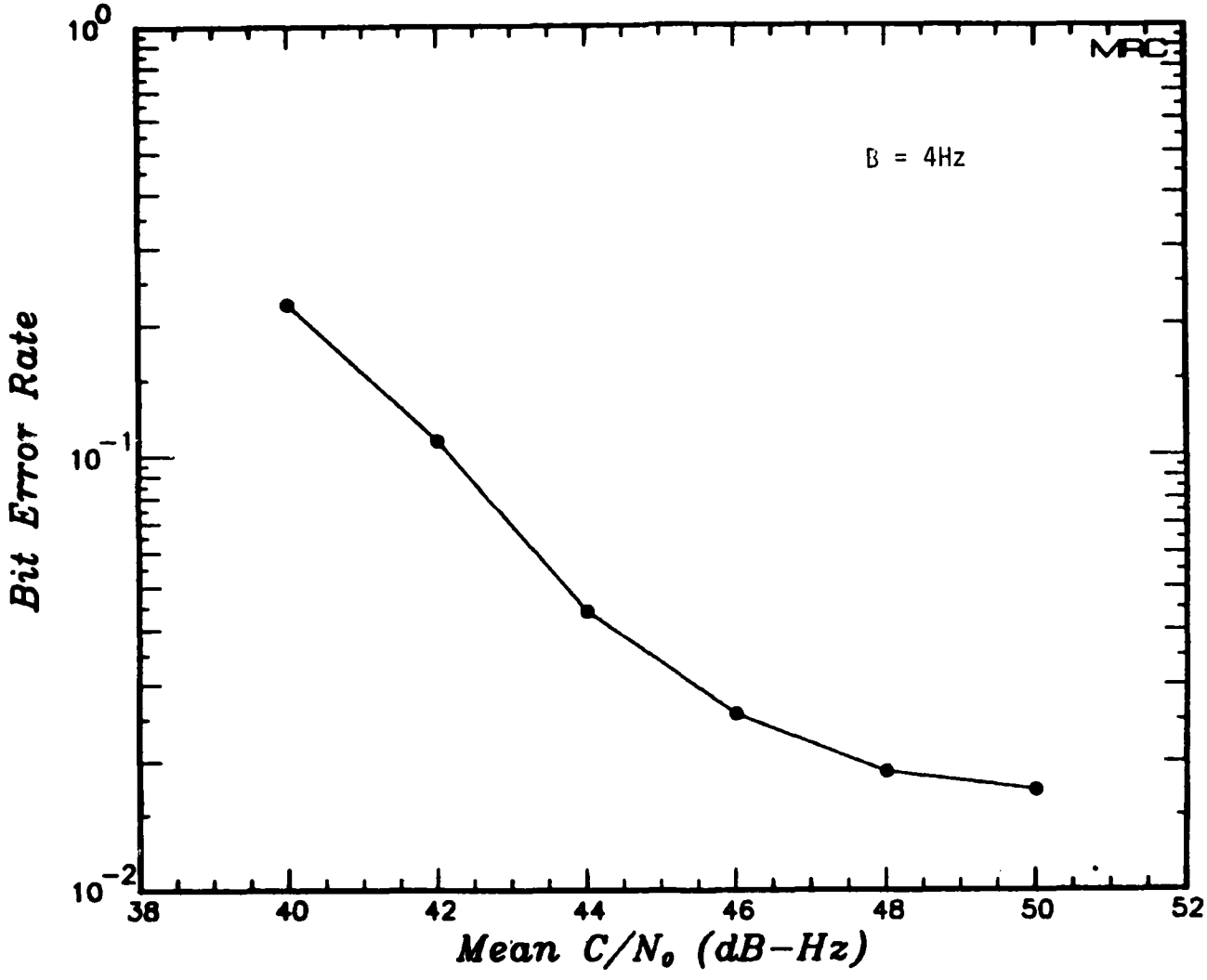

Figure 11. Bit error rate versus $\overline{C}/N_0$ for Receiver Model No. 2 for doppler bandwidth of 4 hertz.

Figure 12 shows the error rate versus $\overline{C}/N_0$ characteristic for several doppler bandwidth values. Figure 13 shows the same data plotted in the form of error rate versus B characteristic curves for several values of $\overline{C}/N_0$. The DFE coefficients misadjustment due to adaptation lag increases with B, and the resulting effects upon the error rates are shown in both of these figures.

4.3 CONCLUSIONS

The adaptive DFE is an effective solution to intersymbol interference if the channel impulse response is constant or very slowly changing. For severe levels of intersymbol interference, the inclusion of adaptive equalization into the link design was shown in Section 4 to be much more beneficial than increasing the received signal-to-noise ratio.

The effectiveness of the adaptive DFE can be limited by the rapidity of channel fluctuations, parameterized in Section 4.2 by the doppler bandwidth B. The specific 2400 baud modem considered in that section exhibited usable channel capacity for values of B up to 4 Hz. For $\overline{C}/N_0$ equal to 44 dB-Hz and B equal to 4 Hz, the measured channel symbol error rate was about 0.04. To make such a modem useful for practical applications one would employ some form of channel symbol error control. Augmenting this modem with rate 1/2, constraint length 7 convolutional coding, interleaving and Viterbi decoding would produce a 1200 band data link with an expected error rate of less than 10^{-3}. Employing rate 1/4 or rate 1/8 codes instead of the rate 1/2 code would yield 600 and 300 baud links with much lower error rates.

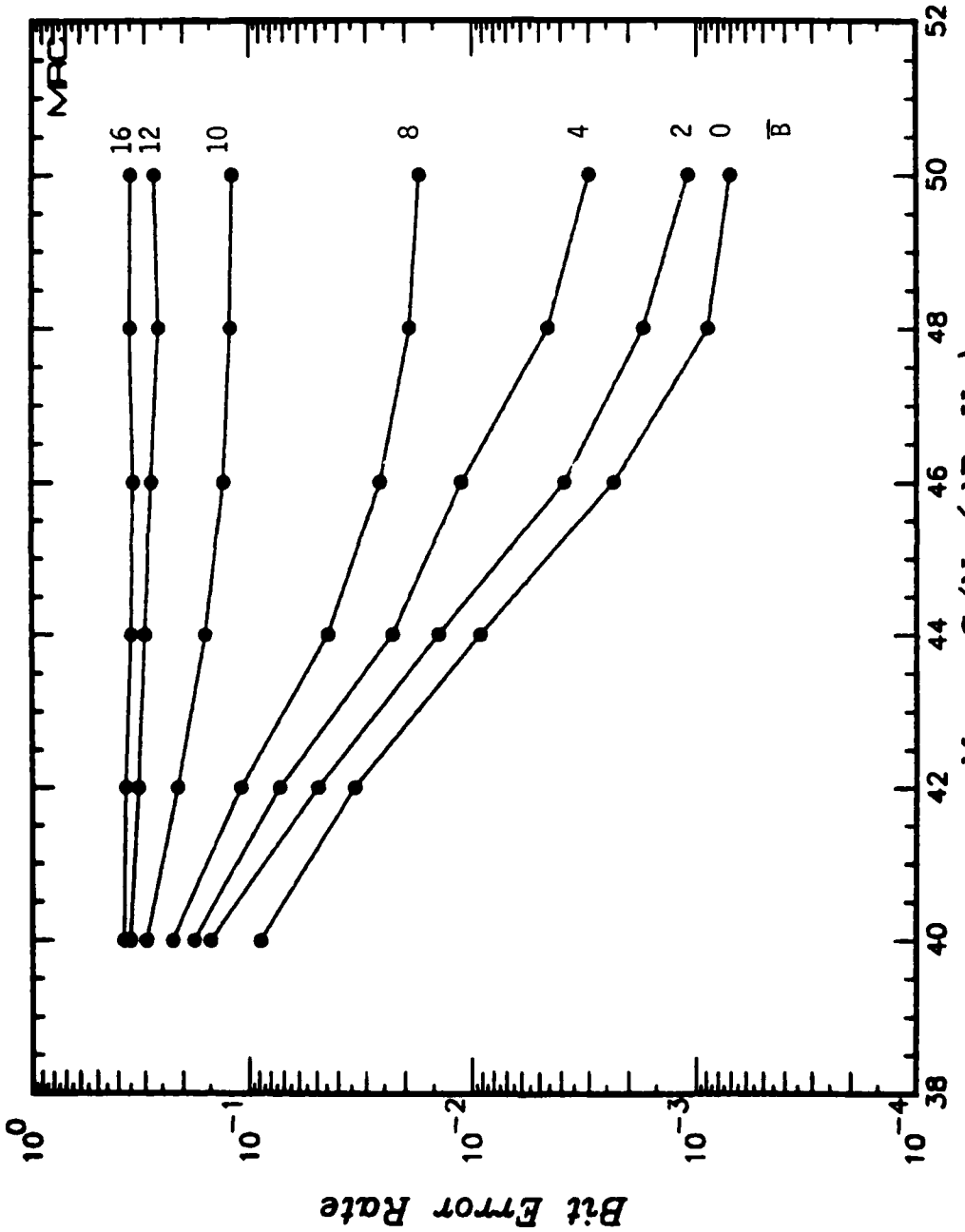

Figure 12. Bit error rate versus $\overline{C}/N_0$ for Receiver Model No. 2 for various doppler bandwidths.

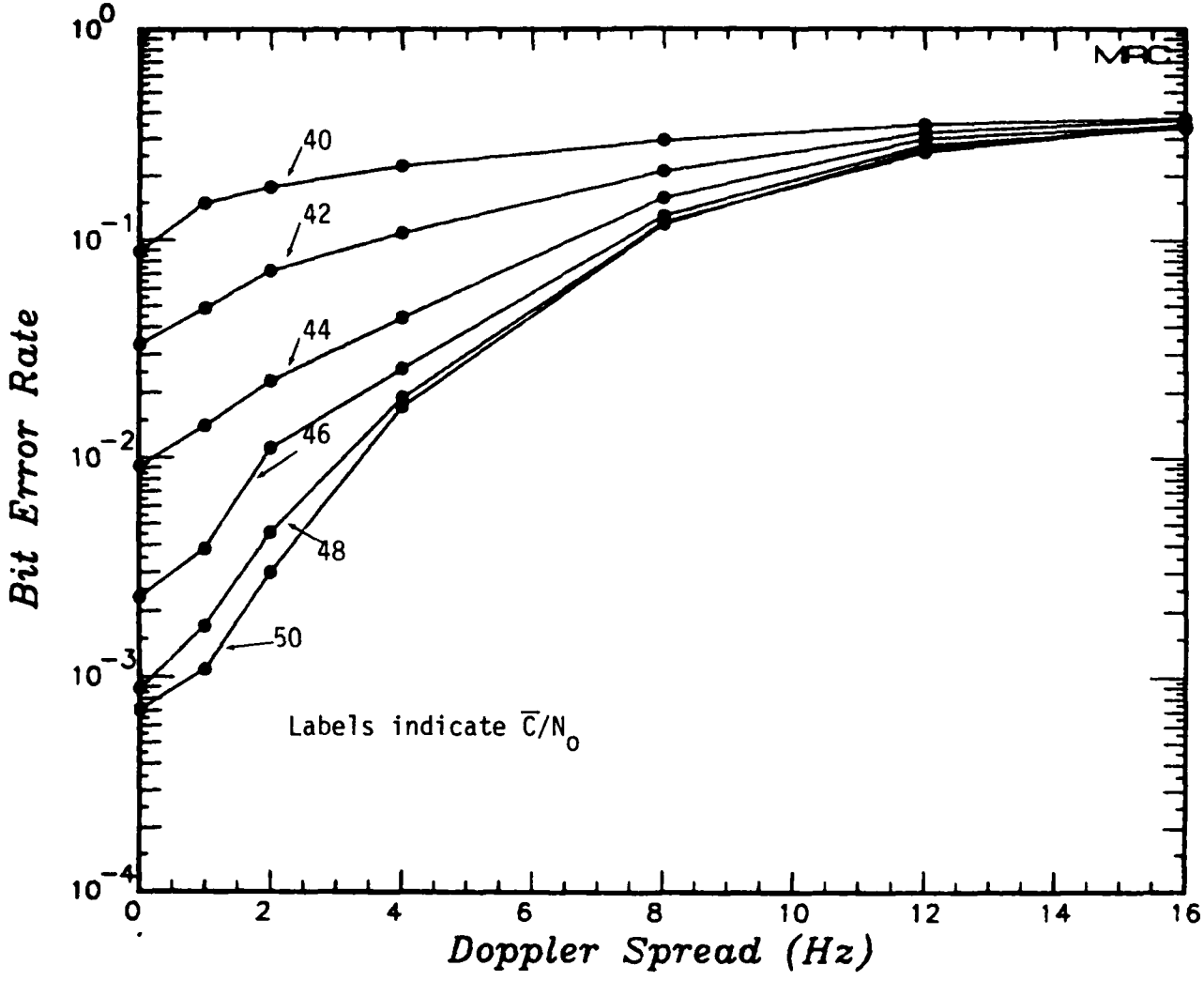

Figure 13. Bit error rate versus doppler bandwidth for various values of $\overline{C}/N_0$.

REFERENCES

1. Austin, M. E., Decision-Feedback Equalization for Digital Communication Over Dispersive Channels, MIT Lincoln Laboratory Technical Report 437, August 1967.

2. Gersho, A., "Adaptive Equalization of Highly Dispersive Channels for Data Transmission," Bell Systems Technical Journal, Vol 48, No. 1, pp. 55-70, January 1969.

3. Godard, D., "Channel Equalization Using a Kalman Filter for Fast Data Transmission," IBM Journal of Research and Development, pp. 561-273, May 1974.

4. Falconer, D. D. and L. Ljung, "Application of Fast Kalman Estimation to Adaptive Equalization," IEEE Transactions on Communications, COM-26, No. 10, pp. 1439-46, October 1978.

5. Ljung, L., M. Morf and D. D. Falconer, "Fast Calculation of Gain Matrices for Recursive Estimation Schemes," Bell Systems Technical Journal of Control, Vol. 27, No. 1, pp. 1-19, January 1978.

6. Mueller, M. S. "Least-Squares Algorithms for Adaptive Equalizers," Bell Systems Technical Journal, Vol. 60, No. 8, pp. 1905-1925, October 1981.

7. Grisdale, G. L., J. G. Morris and D. S. Palmer, "Fading of Long Distance Radio Signals and a Comparison of Space and Polarization Diversity Reception in the 6-18 M c/s Range," Proc. IEE, Vol. 104, Part B., pp 39-51, January 1957.

8. Sifford, B. M., etc., HF Time and Frequency Dispersion Effects - Experimental Validation of an FSK Error-Rate Model, SRI, AD-618330, March 1965.

9. Goldberg, B., "300 KHz-30 MHz MF/HF," IEEE Trans. Commu. Tech., Vol. COM-14, pp 767-784, December 1966.

10. Watterson, C. C., J. R. Juroshek, and W. D. Bensema, "Experimental Confirmation of an HF Channel Model," IEEE Trans. Commun. Technol. COM-18, 792-803, 1970.

11. Rice, D. W., "Phase Characteristics of Ionospherically Propagated Radio Waves," Nature London, 244 (136), 86-88, 1973.

12. Goldberg, B., Communication Channels, Characterization and Behavior, IEEE Press, New York 1975.

13. Bello, P. A., L. W. Pickering, G. E. Peo, and K. P. Jauniskis, Wideband HF Channel Measurements Studies, Project 47, CNR Inc., Needham, Mass., March 1979.

14. Wagner, L. S., J. A. Goldstein and E. A. Chapman, Wideband HF Channel Prober: System Description," NRL Report 8622, March 1983.

15. Findings from the DNA High Altitude Nuclear Effects Summer Study (HF Committee), June 1982.

16. Gutsche, S. L., and M. R. Frolli, Estimates of HF/VHF Signal Characteristics in Nuclear AGW and Plume Scatter Environments, MRC-R-810, January 1984.

DISTRIBUTION LIST

DEPARTMENT OF DEFENSE

Asst to the Sec of Def, Atomic Energy
ATTN: Exec Asst

Defense Advanced Rsch Proj Agency
ATTN: GSD, R. Alewene
ATTN: STO, W. Kurowski

Defense Communications Agency
ATTN: Code 230
ATTN: Code 205
ATTN: J300 for Yen-Sun Fu

Defense Communications Engineer Ctr
ATTN: Code R410
ATTN: Code R510, N. Jones
ATTN: Code R123

Defense Nuclear Agency
ATTN: STNA
ATTN: RAEE
ATTN: NAWE
ATTN: RAAE, P. Lunn
ATTN: NATF
ATTN: RAAE, K. Schwarts
3 cys ATTN: RAAE
4 cys ATTN: STTI-CA

Defense Tech Info Ctr
12 cys ATTN: DD

Dep Under Sec of Def, Comm, Cmd, Cont & Intell
ATTN: Dir of Intell Sys

Field Command, DNA, Det 1
Lawrence Livermore National Lab
ATTN: FC-1

Field Command, Defense Nuclear Agency
ATTN: FCPR
ATTN: FCTXE
ATTN: FCTT, W. Summa

Interservice Nuc Wpns School
ATTN: TTV

Joint Chiefs of Staff
ATTN: C3S
ATTN: C3S Eval Ofc, HDOO

Joint Data System Support Ctr
ATTN: G510, G. Jones
ATTN: C-312, R. Mason
ATTN: G510, P. Bird
ATTN: C-500

Joint Strat Tgt Planning Staff
ATTN: JPPFD
ATTN: JPSS
ATTN: JPTM
ATTN: JLAA
ATTN: JLKS
ATTN: JLK, DNA Rep

National Security Agency
ATTN: B-43, C. Goedeke
ATTN: W-36, O. Bartlett

DEPARTMENT OF DEFENSE (Continued)

Under Sec of Def for Rsch & Engrg
ATTN: Strat & Space Sys (OS)
ATTN: Strat & Theater Nuc forces, B. Stephan

WWMCCS System Engineering Org
ATTN: R. Crawford

DEPARTMENT OF THE ARMY

Asst Ch of Staff for Automation & Comm
ATTN: DAMO-C4, P. Kenny

US Army Comm-Elec Engrg Instal Agency
ATTN: CC-CE-TP, W. Nair

US Army Comm Cmd
ATTN: CC-OPS-WR, H. Wilson
ATTN: CC-OPS-W

US Army Comm R&D Cmd
ATTN: DRDCO-COM-RY, W. Kesselman

DEPARTMENT OF THE NAVY

Naval Electronic Systems Command
ATTN: Code 501A
ATTN: Code 3101, T. Hughes
ATTN: PME 117-20
ATTN: PME 106-4, S. Kearney
ATTN: PME 117-211, B. Kruger
ATTN: PME-117-2013, G. Burnhart
ATTN: PME-106, F. Diederich

Naval Ocean Systems Ctr
ATTN: Code 5323, J. Ferguson
ATTN: Code 5322, M. Paulson
ATTN: Code 532

Naval Rsch Laboratory
ATTN: Code 4720, J. Davis
ATTN: Code 4700, S. Ossakow
ATTN: Code 7500, B. Wald
ATTN: Code 4780
ATTN: Code 4700
ATTN: Code 4187
ATTN: Code 7950, J. Goodman
ATTN: Code 6700
ATTN: Code 4108, E. Szuszewicz

Naval Telecommunications Command
ATTN: Code 341

Ofc of the Dep Ch of Naval Ops
ATTN: NOP 981N
ATTN: NOP 941D
ATTN: NOP 654, Strat Eval & Anal Br

Ofc of Naval Rsch
ATTN: Code 412, W. Condell

DEPARTMENT OF THE AIR FORCE

Air Force Geophysics Laboratory
ATTN: OPR-1
ATTN: LIS, J. Buchau

DEPARTMENT OF THE AIR FORCE (Continued)

Dep Ch of Staff, Rsch, Def & Acq
ATTN: AFRDS, Space Sys & C3 Dir

Dep Ch of Staff, Plans & Opns
ATTN: AFXOKCD
ATTN: AFXOKS
ATTN: AFXOKT

Electronic Systems Div
ATTN: SCS-2, G. Vinkels
ATTN: SCS-1E

Rome Air Development Ctr
ATTN: TSLD
ATTN: OCSA, R. Schneible
ATTN: OCS, V. Coyne

Rome Air Development Center
ATTN: EEP, J. Rasmussen
ATTN: EEPS, P. Kossey

Space Command
ATTN: DC, T. Long

Strategic Air Command
ATTN: ADWA
ATTN: DCX
ATTN: DCZ
ATTN: NRI/STINFO Library
ATTN: XPFC
ATTN: XPFS
ATTN: XPQ

OTHER GOVERNMENT AGENCY

Institute for Telecommunications Sciences
ATTN: A. Jean
ATTN: L. Berry
ATTN: W. Utlaut

NATO

NATO School, SHAPE
ATTN: US Documents Officer

DEPARTMENT OF ENERGY CONTRACTORS

University of California
Lawrence Livermore National Lab
ATTN: L-31, R. Hager
ATTN: Tech Info Dept Library

Los Alamos National Laboratory
ATTN: D. Sappenfield
ATTN: J. Wolcott
ATTN: R. Jeffries
ATTN: P. Keaton
ATTN: D. Simons
ATTN: G-6, E. Jones
ATTN: MS 664, J. Zinn
ATTN. J. Hopkins
ATTN: T. Kunkle, ESS-5

DEPARTMENT OF DEFENSE CONTRACTORS

Aerospace Corp
ATTN: S. Mewaters

Analytical Systems Engineering Corp
ATTN: Security

DEPARTMENT OF DEFENSE CONTRACTORS (Continued)

Aerospace Corp
ATTN: J. Kluck
ATTN: I. Garfunkel
ATTN: D. Olsen
ATTN: J. Straus
ATTN: R. Slaughter
ATTN: T. Salmi
ATTN: V. Josephson
ATTN: E. Rodriguez
ATTN: K. Cho
ATTN: D. Whelan

Analytical Systems Engineering Corp
ATTN: Radio Sciences

Austin Research Assoc
ATTN: J. Thompson
ATTN: B. Moore
ATTN: M. Sloan
ATTN: J. Uglum

BDM Corp
ATTN: L. Jacobs
ATTN: T. Neighbors

Berkeley Rsch Associates, Inc
ATTN: J. Workman
ATTN: C. Prettie
ATTN: S. Brecht

BR Communications
ATTN: J. McLaughlin

University of California
ATTN: H. Booker

California Rsch & Tech, Inc
ATTN: M. Rosenblatt

Communications Satellite Corp
ATTN: G. Hyde
ATTN: D. Fang

EOS Technologies, Inc
ATTN: B. Gabbard
ATTN: W. Lelevier

GTE Communications Products Corp
ATTN: H. Gelman
ATTN: A. Murphy

GTE Govt Systems Corp
ATTN: R. Steinhoff

Harris Corp
ATTN: E. Knick

IBM Corp
ATTN: H. Ulander

Institute for Defense Analyses
ATTN: E. Bauer
ATTN: H. Wolfhard
ATTN: J. Aein
ATTN: H. Gates

ITT Corp
ATTN: G. Wetmore

DEPARTMENT OF DEFENSE CONTRACTORS (Continued)

ITT Corp
ATTN: Tech Library

Kaman Sciences Corp
ATTN: E. Conrad

Kaman Tempo
ATTN: DASIAC

Kaman Tempo
ATTN: B. Gambill
ATTN: DASIAC
ATTN: W. McNamara

M/A Com Linkabit Inc
ATTN: I. Jacobs
ATTN: H. Van Trees
ATTN: A. Viterbi

Magnavox Govt & Indus Electronics Co
ATTN: G. White

Maxim Technologies, Inc
ATTN: J. Marshall
ATTN: F. Tsui
ATTN: R. Morganstern

Meteor Communications Corp
ATTN: R. Leader

Mission Research Corp
ATTN: G. McCartor
ATTN: F. Guigliano
ATTN: Tech Library
ATTN: F. Fajen
ATTN: R. Bogusch
ATTN: R. Hendrick
ATTN: D. Knepp
ATTN: R. Kilb
ATTN: S. Gutsche
ATTN: R. Dana
ATTN: C. Lauer
ATTN: R. Bigoni
2 cys ATTN: B. Sawyer
5 cys ATTN: Doc Control

DEPARTMENT OF DEFENSE CONTRACTORS (Continued)

Mitre Corp
ATTN: A. Kymmel
ATTN: G. Harding
ATTN: MS J104, M. Dresp
ATTN: C. Callahan

Mitre Corp
ATTN: W. Hall
ATTN: W. Foster
ATTN: J. Wheeler
ATTN: M. Horrocks

Physical Dynamics, Inc
ATTN: E. Fremouw
ATTN: J. Secan

R&D Associates
ATTN: M. Gantsweg
ATTN: C. Greifinger
ATTN: F. Gilmore
ATTN: H. Ory
ATTN: R. Turco
ATTN: W. Wright
ATTN: W. Karzas
ATTN: G. Stcyr
ATTN: P. Haas

Rockwell International Corp
ATTN: S. Quilici

SRI International
ATTN: C. Rino
ATTN: D. Neilson
ATTN: D. McDaniels
ATTN: R. Leadabrand
ATTN: V. Gonzales
ATTN: W. Jaye
ATTN: G. Price
ATTN: R. Tsunoda
ATTN: J. Vickrey
ATTN: G. Smith

END

FILMED

9-85

DTIC